Available online at www.sciencedirect.com
SCIENCE DIRECT®
International Journal of Plasticity 22 (2006) 1610–1657
INTERNATIONAL JOURNAL OF Plasticity
www.elsevier.com/locate/ijplas

Nonlinear dependence of viscosity in modeling the rate-dependent response of natural and high damping rubbers in compression and shear: Experimental identification and numerical verification

A.F.M.S. Amin [a], A. Lion [b], S. Sekita [c], Y. Okui [c,*]

[a] *Department of Civil Engineering, Bangladesh University of Engineering and Technology, Dhaka 1000, Bangladesh*
[b] *Institute of Mechanics, University of Kassel, Mönchebergstrasse 7, Kassel 34107, Germany*
[c] *Department of Civil and Environmental Engineering, Saitama University, 255 Shimo Okubo, Saitama 338-8570, Japan*

Received 24 February 2005
Available online 9 December 2005

Abstract

The rate-dependent behavior of filled natural rubber (NR) and high damping rubber (HDR) is investigated in compression and shear regimes. In order to describe the viscosity-induced rate-dependent effects, a constitutive model of finite strain viscoelasticity founded on the basis of the multiplicative decomposition of the deformation gradient tensor into elastic and inelastic parts is proposed. The total stress is decomposed into an equilibrium stress and a viscosity-induced overstress by following the concept of the Zener model. To identify the constitutive equation for the viscosity from direct experimental observations, an analytical scheme that ascertains the fundamental relation between the inelastic strain rate and the overstress tensor of the Mandel type by evaluating simple relaxation test results is proposed. Evaluation of the experimental results using the proposed analytical scheme confirms the necessity of considering both the current overstress and the current deformation as variables to describe the evolution of the rate-dependent phenomena. Based on this experimentally based motivation, an evolution equation using power laws is proposed to represent the effects of internal variables on viscosity phenomena. The proposed evolution equation has been incorporated in the finite strain viscoelasticity model in a thermodynamically consistent way.

* Corresponding author. Tel.: +81 48 858 3558; fax: +81 48 858 7374.
E-mail address: okui@post.saitama-u.ac.jp (Y. Okui).

0749-6419/$ - see front matter
doi:10.1016/j.ijplas.2005.09.005

Simulation results for simple relaxation tests, multi-step relaxation tests and monotonic tests at different strain rates using the developed model show an encouraging correlation with the experiments conducted on HDR and NR in both compression and shear regimes. Finally, an approach to extend the proposed evolution equation for rate-dependent cyclic processes is proposed. The simulation results are critically compared with the experiments.

Keywords: A: Stress relaxation; B: Polymeric material; C: Mechanical testing; B: Constitutive behavior; Viscoelasticity

1. Introduction

1.1. General

Vulcanized rubbers are one of the most remarkable materials having a wide range of engineering applications including tires, engine mounts, shock-absorbing bushes, seals, tunnel linings and wind shoes (Roeder and Stanton, 1983; Ward, 1985; Mullins, 1987; Castellani et al., 1998). Special fillers, for example, carbon black or silica are usually added during vulcanization for improving the strength and toughness properties of rubber to suit these individual applications (Wischt, 1998). The recent development of high damping rubber (HDR) in base isolation devices for protecting buildings and bridges from devastating earthquakes is another emerging dimension of engineering applications of rubber (see Fujita et al., 1990; Kelly, 1991; Carr et al., 1996; Mori et al., 1996; Dorfmann and Burtscher, 2000). Rubber industries follow a special vulcanization procedure to produce HDR. Bridges and buildings with HDR base isolation devices have so far been displayed encouraging field level performances by sustaining severe shocks during Loma Prieta (1989), Northridge (1994) and Kobe (1995) earthquakes (Kelly, 1997). Rubber bearings for base isolation devices are usually made of thin horizontal rubber layers bonded with alternately placed horizontal steel plates (Roeder and Stanton, 1983). Cubic and cylindrical shapes are the most common geometries for rubber bearings. Yet the other variations may include trapezoidal or tapered shapes (AASHTO, 1992; Ramberger, 2002; Mattheck and Erb, 1991) and also having V-shaped steel plates (European Commission, 1999). In base isolation devices, steel plates imply large stiffness under vertical loadings, while rubber layers incorporate low horizontal stiffness when the structure is subjected to lateral loads (e.g., earthquakes, wind, etc.). Usually, the bearings remain under compression due to the gravity loads coming from the superstructures. However, compression and shear deformations act together on these bearings when a lateral load like wind or an earthquake strikes. To estimate the performance of the bearings and thereby finding their optimum design, the engineers usually deal with test data obtained from expensive tests conducted on prototypes or full scale specimens. On the other hand, there exists another possibility to develop a reliable numerical procedure like the finite element method for predicting the performance. Nevertheless, the core of such a general numerical procedure depends largely on the constitutive model that is adequate enough for describing the major phenomena of HDR in the relevant deformation range.

Under compression and shear deformations, HDR is expected to exhibit a high stiffness under low strains so that motions of the structure due to service loads, traffic and wind

become as low as possible. However, when the structure is subjected to large cyclic or stochastic loads arising from earthquakes, the base isolation system should facilitate the absorption of the delivered energy through its hysteresis properties. To achieve all these features in HDR, a large amount of fillers (about 30%) including carbon black, silica, oils and some other particles is added during the vulcanization process (Kelly, 1997; Yoshida et al., 2004). Thus, HDR is developed to exhibit a strong nonlinear rate-dependent response under monotonic loadings and to show significant hysteresis effects or energy dissipation during cyclic loads. Recently, Amin (2001) and Amin et al. (2006) studied the nonlinear rate-independent monotonic behavior of the equilibrium stress of HDR under compression and shear. In these studies, an improved hyperelasticity relation, a procedure for the identification of its material parameters and the implementation of the model in a general purpose finite element code have been proposed to simulate rate-independent responses. A study on modeling the quasi-static cyclic behavior of HDR under shear is recently reported in Yoshida et al. (2004). All these studies, however, revealed the existence of significant rate-dependence phenomena in HDR. This emphasizes the need for a thorough experimental characterization and the development of modeling techniques for rate-dependent behavior. The current work addresses these aspects.

1.2. Rate-dependent phenomena in rubbers and constitutive modeling

The experimental study of the effect of strain-rate on the response of filled rubber dates back to the early sixties when the tensile strength of rubber was found to increase with increasing strain rate (Mason, 1960; Dannis, 1962). The appearance of this property possesses an inherent relation to the presence of carbon black in the rubber matrix. Yet, the effect of the strain-rate on a material is better studied through relaxation tests when the specimen is subjected to constant strains and the corresponding stress responses are recorded. In this context, Gent (1962a,b) noted that the stress in the specimens subjected to constant strains relaxes significantly during the first two seconds. However, his experimental arrangements did not allow him to make measurements in time intervals less than 6 s. Owing to this reason, the time history of the stress relaxation during the first six seconds of the tests remained unknown. However, the advent and use of high-speed digital computers in data acquisition systems has helped to a great extent. With the aid of digital data acquisition systems, the subsequent studies of Lion (1996), Bergström and Boyce (1998, 2000) report more detail information about the relaxation history of rubbers under uniaxial tension and compression. Miehe and Keck (2000) studied the relaxation phenomena in uniaxial tension–compression, while Haupt and Sedlan (2001) investigated the phenomena in uniaxial and biaxial tension–torsion deformation modes. Khan and Zhang (2001) investigated the creep, relaxation and rate-dependent behavior of polymers under tension. Other recent experimental studies on the strain-rate effect and relaxation phenomena of different polymers are also available in Colak (2005), Makradi et al. (2005), Khan and Lopez-Pamies (2002), Krempl and Khan (2003). However, experimental information on relaxation phenomena of HDR is limited, whereas no report exists on such a behavior in the shear regime. Amin (2001) and Amin et al. (2002) reported the experimental investigation of HDR in the compression regime and compared the relaxation phenomena with other natural rubber (NR) specimens. When compared with NR, rate-dependence and stress relaxation are much more pronounced in HDR. Upon review of the results of available experimental studies, there comes out the opinion that relaxation processes in rubber

usually involve a very fast rate of stress decay during the first few seconds. It is followed by a very slow rate in the long-term range. The HDR shows such an effect in a prominent way. The vulcanization process usually bears a significant influence on the appearance of such relaxation phenomena (Ward, 1985; Mason, 1960; Meinecke and Taftaf, 1987; Wischt, 1998).

Modeling of rate-dependent phenomena in elastomers is, perhaps, one of the most intricate tasks for the rheologists of present day (Bardenhagen et al., 1997). Due to the presence of high deformability and strong nonlinearities, the constitutive model needs to be founded on finite strain theories in consistence with the natural laws of thermodynamics. To model viscoelastic material behavior under finite deformations there are, in principle, two different approaches which can be motivated from the theory of linear viscoelasticity under small strains. The first approach generalizes the concept of the Zener model or, more general, the concept of Maxwell chains consisting of n elements to three-dimensional finite deformations. In this case, the framework of multiplicative inelasticity leads to a set of n multiplicative decompositions of the deformation gradient in parallel. The fundamental advantages of this concept are that each decomposition is independent from the others and that the material model can easily be extended by adding additional Maxwell elements. Naturally, the approach of Maxwell elements is applied to formulate constitutive models where the deformation history is the independent and the current stress the dependent variable. The second approach corresponds to the generalization of the Poynting–Thomson model or, more general, to the generalization of Kelvin chains with n elements to finite deformations. In this case, one would obtain n intermediate configurations or decompositions of the deformation gradient, where each of them depends on all the others. In linear viscoelasticity this approach is mainly used to develop material models, where the stress history is the independent and the current strain the dependent variable. Further discussions of the Zener and the Poynting–Thomson models are available in Huber and Tsakmakis (2000a) and Laiarinandrasana et al. (2003). In order to formulate the constitutive theory as simple as possible, in this paper, we take the choice of the generalization of the Zener model to finite strains as illustrated in Fig. 1.

A large number of models of finite viscoelasticity is based on a phenomenological approach, whereas some interesting models based on micromechanics also appeared until very recently. When both the approaches have their own possibilities, the limited availability of information regarding the microstructure and the composition of HDR motivates the current work to consider the phenomenological approach. For micromechanics-based

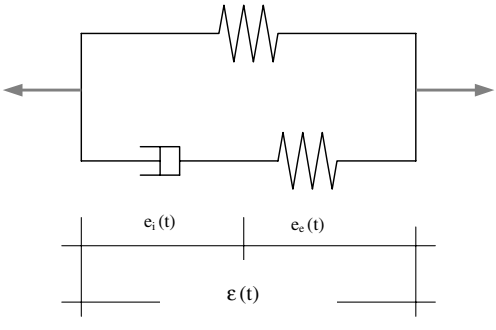

Fig. 1. Zener model.

approaches, the readers may refer to Ball et al. (1981), Bergström and Boyce (1998, 2000), Drozdov and Dorfmann (2003) and the references cited therein.

The constitutive theory of finite linear viscoelasticity (Coleman and Noll, 1960, 1961) is a major foundation for modeling rate-dependent material behavior based on the phenomenological approach. This general theory is formulated using functionals with fading memory properties. Sullivan et al. (1979), Johnson and Stacer (1993), Johnson et al. (1993, 1994) and Quigley and Mead (1995) proposed simplified versions of the general theory. In these theories, the stress is decomposed into an equilibrium stress that corresponds to the stress response at an infinite slow rate of deformation and a viscosity-induced overstress. The overstress is expressed as an integral over the deformation history and a relaxation function is specified as a measure for the material's memory (Christensen, 1980; Simo, 1987; Drozdov, 1997; Holzapfel and Simo, 1996; Holzapfel, 1996; Kaliske and Rothert, 1997). The thermodynamic consistency requires the relaxation function to be positive with negative slope and to possess a positive curvature (Haupt and Lion, 2002). Within this restriction, for example, an exponential function can be employed (Leonov, 1976). Yet, there exists a considerable limitation in representing the long-term relaxation behavior of rubber using a single exponential function. In this situation, a certain number of decreasing exponentials can be superimposed, referred as a so-called Prony series. This process may invite a large number of material parameters in the model that are difficult to estimate. Another innovative approach (Haupt and Lion, 2002) uses compact relaxation functions based on power laws, for example, the Mittag–Leffler function as also employed in Lion and Kardelky (2004) in describing Payne effect, and involves only a very few number of material parameters. This may have a benefit from the point of view of parameter estimation, but needs to be examined with real test data.

In comparison with this, there exists another possibility of constructing finite strain models of viscoelasticity by considering the multiplicative decomposition of the deformation gradient into elastic and inelastic parts, originally proposed by Green and Tobolsky (1946) and further explored later on by Sidoroff (1975a,b) and Lubliner (1985). The free energy of the system splits additively into equilibrium and non-equilibrium parts giving the elastic equilibrium stress and the viscosity-induced overstress (Huber and Tsakmakis, 2000a). The current paper follows this approach as with earlier works of Lion (1997), Reese and Govindjee (1998), Bonet (2001), and Laiarinandrasana et al. (2003). In this approach, a suitable hyperelasticity model (Mooney, 1940; Rivlin, 1948; Boyce and Arruda, 2000; Seibert and Schöche, 2000) is employed to reproduce the elastic responses represented by the springs, while the dashpot represents the inelastic or the so-called internal strain. Its temporal behavior is determined by an evolution equation that is consistent with the second law of thermodynamics (Huber and Tsakmakis, 2000a,b). A linear relation between the inelastic strain rate and the overstress is assumed as the simplest form of the evolution equation. Yet, such a linear relation does not often hold as other constitutive quantities may influence the overstress dependence of the inelastic strain rate (Krempl, 1987; Amin et al., 2002). Depending on both the material and the experimental results, nonlinear evolution equations are frequently employed to describe this relation. The evolution laws belonging to this class are ordinary differential equations with variable coefficients that depend on the relevant process or internal variables. The structure and thermodynamic consistency of these rate equations based on internal variables are addressed in Coleman and Gurtin (1967), Lubliner (1969, 1973). Based on these papers, Reese and Govindjee (1998), Holzapfel (1996), Miehe and Keck (2000), and Haupt and

Sedlan (2001) attempted to introduce different forms of nonlinear evolution equations to describe the experimentally observed material phenomena. However, in these publications the adoption of different internal variables and their functional relations in the rate equation are based upon theoretical assumptions putting their physical significance into question. Thus, all these models could get a better physical insight into the material if the driving motivations behind developing these functions could be evaluated based on experimental observations. The parameters identified in this way are supposed to bear a better physical understanding of the phenomena.

1.3. Objectives and methodology

The present paper examines the relaxation behavior of HDR under homogeneous states of compression and simple shear. To this end, simple and multi-step relaxation tests were carried out. Identical tests were also carried out with NR for comparison. This paper follows the model of finite strain viscoelasticity presented by Huber and Tsakmakis (2000a,b) in a sense. However, we attempt to show the possibilities of generalizing the viscosity law in a thermodynamically consistent way for the real materials based on experimental observations. To this end, a scheme is proposed to evaluate the relation between the inelastic strain rate and the overstress using experimental data and thereby obtaining the physical motivation of identifying the internal variables and the resulting form of the evolution equation. The equation has been developed by evaluating experimental results under one-dimensional states of stress and strain and subsequently generalized for the three-dimensional case for adoption in finite strain models. One single set of parameters that can represent the relaxation behavior of the material under both compression and shear is identified. The resulting finite strain viscoelasticity model has been used to simulate the material response due to different rate dependent input histories including monotonic as well as simple and multi-step relaxation tests. In order to discuss the capability of the developed theory, the stress responses simulated by the model have been compared with experimental data. Finally, an approach has been proposed to extend the evolution equation for modeling the rate-dependent cyclic behavior of HDR and NR based on the observation that indicated the presence of a significant rate dependence during loading and a weak rate dependence during unloading.

2. Experiments

HDR and NR specimens were tested under compression and simple shear which are the most relevant deformation modes in the application of base isolation bearings. The specimens of NR and HDR have shear moduli (JIS K6301)[1] of about 0.98 and 0.78 MPa and were manufactured by the Yokohama Rubber Company, Japan. HDR contains a much larger amount of fillers/additives than NR. The tests were carried out using a computer-controlled servo hydraulic testing machine (Shimadzu Servo Pulser 4800) with a 200 kN load cell. The maximum displacement rate of the load cell cross-head was 50 mm/s. The displacement was applied in the vertical direction of the specimen and the force response was measured by the load cell. The specimens used

[1] A method recommended by Japanese Standards Association.

for compression tests were cylindrical in shape, i.e. 41 mm in height and 49 mm in diameter. Since a lubricant and a poly-propylene sheet were used to reduce platen-specimen friction, it was possible to obtain a nearly homogeneous uniaxial state of compression. The simple shear specimens (25 mm × 25 mm × 5 mm) had a net shear area of 25 mm × 25 mm. Dual lap shear specimens (Charlton et al., 1994) were used. All tests were carried out at room temperature. Further details of the test set-ups and procedures are described in Amin (2001), Amin et al. (2002, 2003) and Wiraguna (2003). Prior to an actual test, each virgin specimen was subjected to a five-cycle preloading process to remove the Mullins' softening effect (Mullins, 1969). In recent literatures, there are some promising models for representing Mullins' effect (Govindjee and Simo, 1991, 1992a,b;

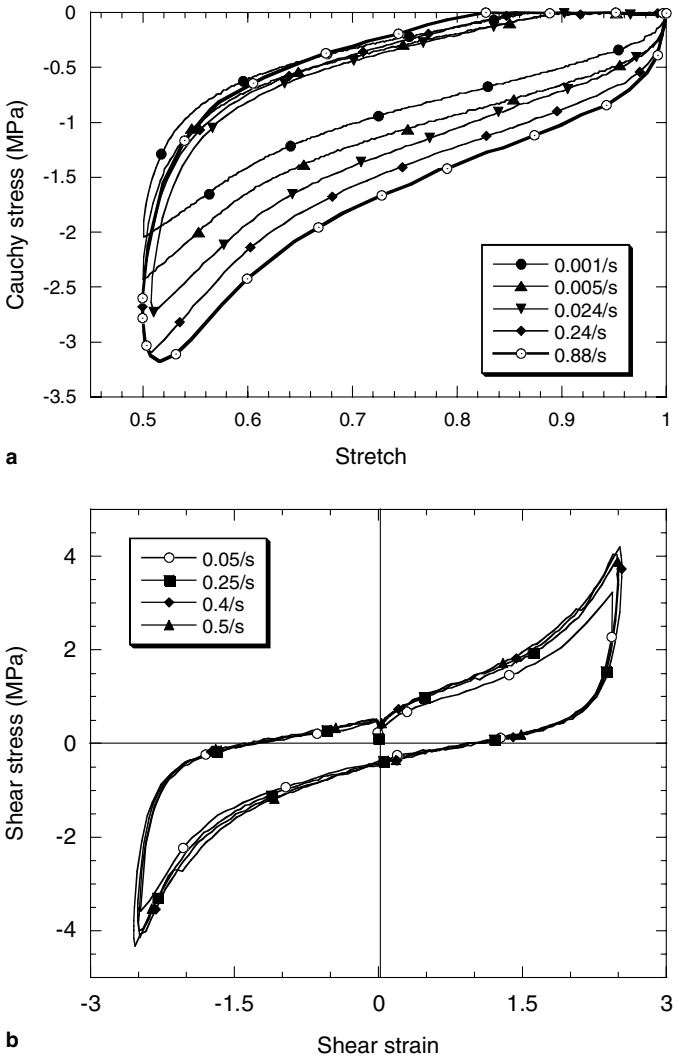

Fig. 2. Cyclic responses obtained from HDR at different strain rates: (a) compression; (b) simple shear. Stress and strain measures are further illustrated in Fig. 13.

Johnson and Beatty, 1993a,b; Ogden and Roxburgh, 1999; Besdo and Ihlemann, 2003a,b), but this paper does not consider such a behavior. This approach of removing Mullins' effect from other phenomena of interest is similar to that of Yeoh (1990), Yamashita and Kawabata (1992), Lion (1996, 1997), Bergström and Boyce (1998) and Miehe and Keck (2000). In preloading for compression tests, a strain rate of 0.01/s was applied for each cycle with a maximum stretch of 0.5. In the shear specimens, the strain rate applied during the cyclic process up to 2.5 shear strain was 0.05/s. All tests were conducted 20 min after completing the preloading to regularize the healing effect (Bueche, 1961) that can exist in the specimens. Each test was conducted with a new specimen that only contained the history of the preloading procedure.

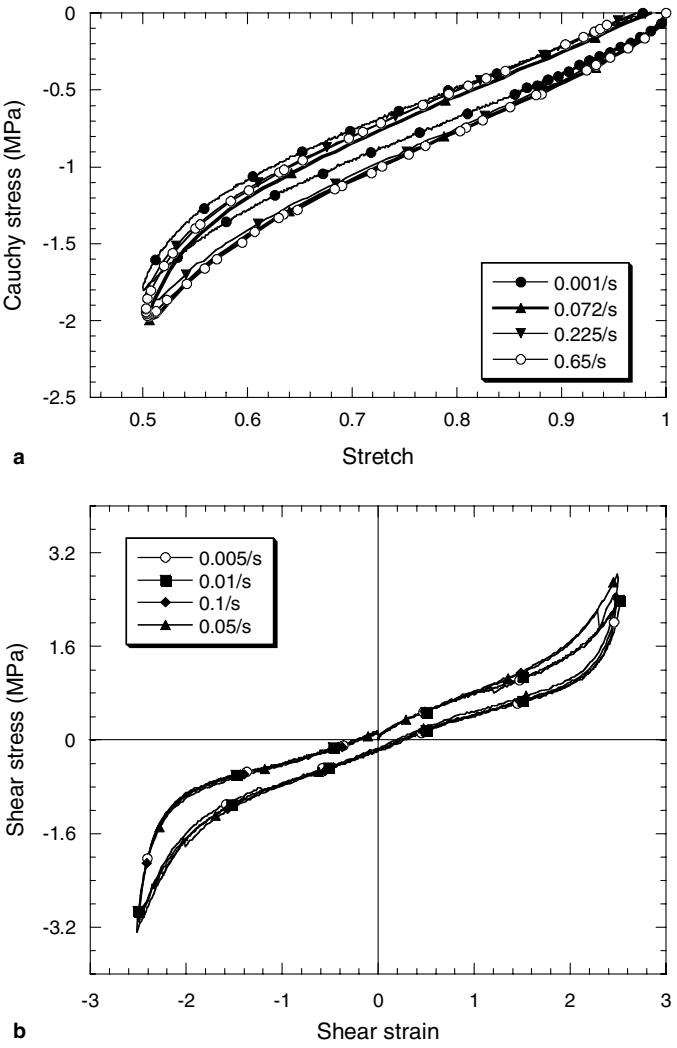

Fig. 3. Cyclic responses obtained from NR at different strain rates: (a) compression; (b) simple shear. Stress and strain measures are further illustrated in Fig. 13.

2.1. Cyclic tests at different strain rates

To study the rate-dependence, HDR and NR specimens were subjected to cyclic processes with constant strain rates. The strain rates applied in these tests have been calculated in terms of the initial dimension of the specimen measured just before the respective test. Fig. 2 presents the stress–strain responses as obtained from HDR under cyclic compression and shear deformations. Five tests were conducted in compression, each with a particular strain rate. In shear, four tests were carried out. The monotonic responses as visible from the tests are found to be strongly nonlinear at low, moderate and high strain levels. A comparison of the stress responses indicates a strongly pronounced rate-dependent behavior during loading, whereas a much weaker rate-dependence is observed during unloading. In addition, the presence of hysteresis along with

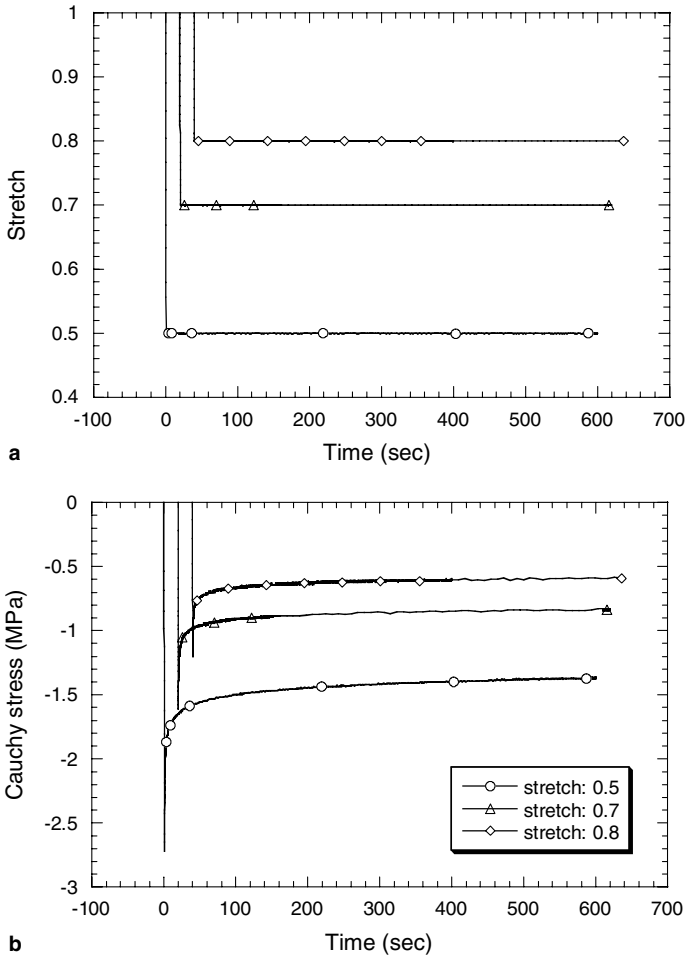

Fig. 4. Simple relaxation tests conducted on HDR at different stretch levels in compression regime: (a) applied stretch history; (b) stress history. For the purpose of understandable illustration, the stretch and stress histories have been separated from each other by 20 s. Stress and strain measures are further illustrated in Fig. 13.

permanent set is visible. The corresponding observations on NR are presented in Fig. 3, where rate-dependence, hysteresis and permanent set are found to be much lower than in the case of HDR. The presence of a lower filler content in NR is a major factor behind such a display. In this context, we note an earlier report (Bergström and Boyce, 1998), where also a weak rate-dependence during unloading has been observed in samples containing high filler contents. The hysteresis and permanent set effects are related to slip processes between adjacent filler particles in the rubber microstructure (Kilian et al., 1994), thus breaking the rubber–filler bonds that are healable (Bueche, 1961). The effect will be further discussed in the following section along with the results of simple relaxation tests. In general, all responses during loading suggest a diminishing trend in the increase of the stress with increasing strain rate. Such a behavior can be related to the approach of the material towards the so-called instantaneous stress response as

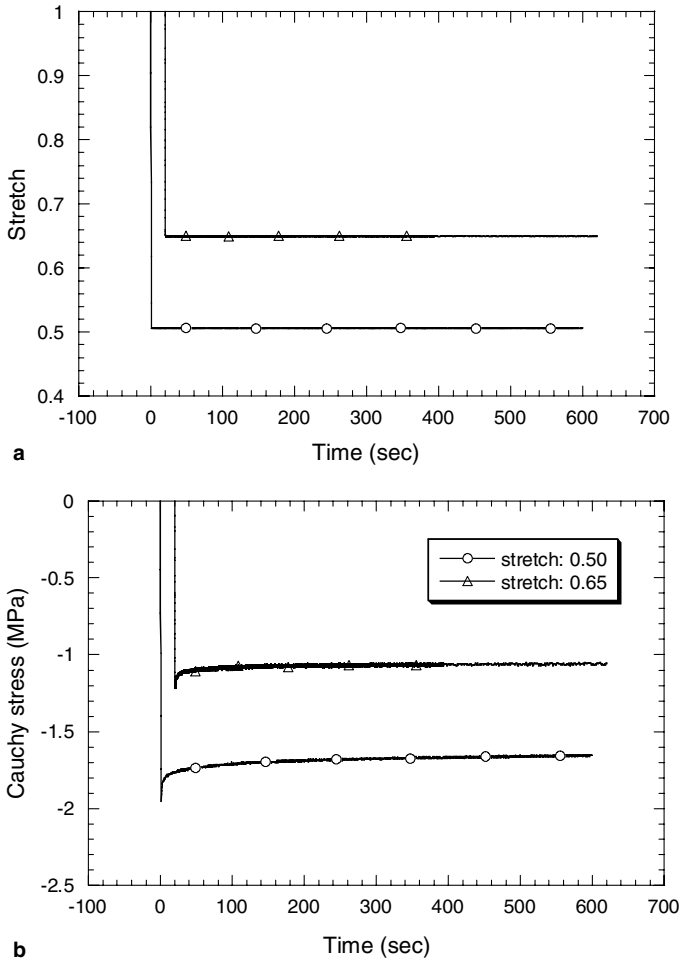

Fig. 5. Simple relaxation tests conducted on NR at different stretch levels in compression regime: (a) applied stretch history; (b) stress history. For the purpose of understandable illustration, the stretch and stress histories have been separated from each other by 20 s. Stress and strain measures are further illustrated in Fig. 13.

observed earlier in the compression regime (see Amin et al., 2002), but confirmed here also in shear regime.

2.2. Relaxation tests

The stress responses obtained from cyclic strain-controlled tests at different strain rates have shown a strong rate dependence during loading and a less rate dependence during unloading. In terms of a phenomenological interpretation, the viscosity of the material can be attributed to this type of material behavior. To this end, the relaxation behavior induced by the viscosity at different strain levels is examined in detail through simple and multi-step relaxation tests (Figs. 4(a), 5(a), 6(a), 7(a) and 8). In the compression tests,

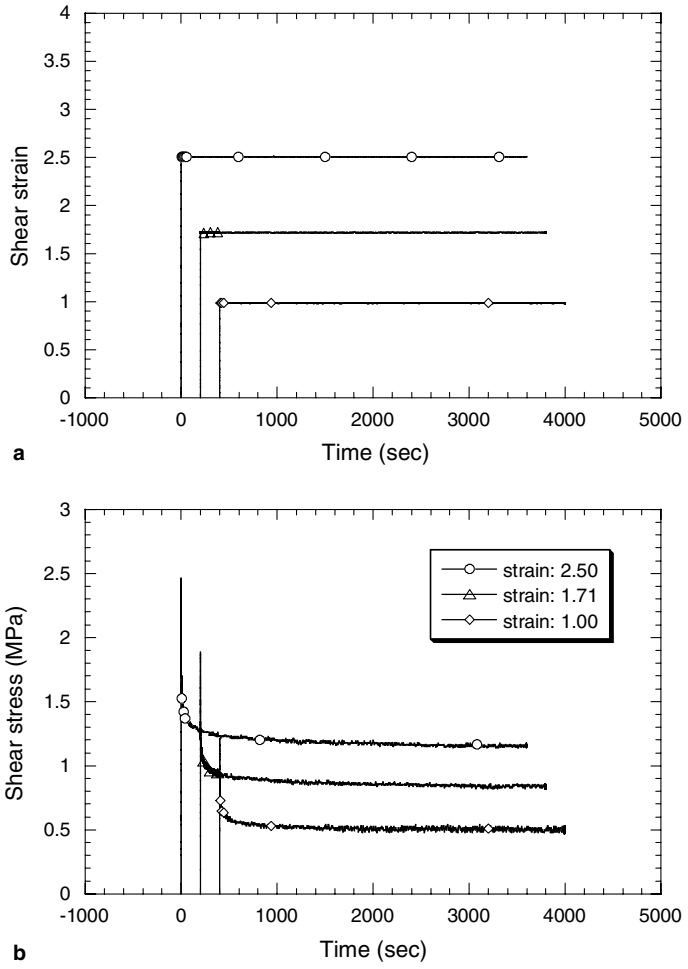

Fig. 6. Simple relaxation tests conducted on HDR at different strain levels in shear regime: (a) applied strain history; (b) stress history. For the purpose of understandable illustration, the strain and stress histories have been separated from each other by 100 s. Stress and strain measures are further illustrated in Fig. 13.

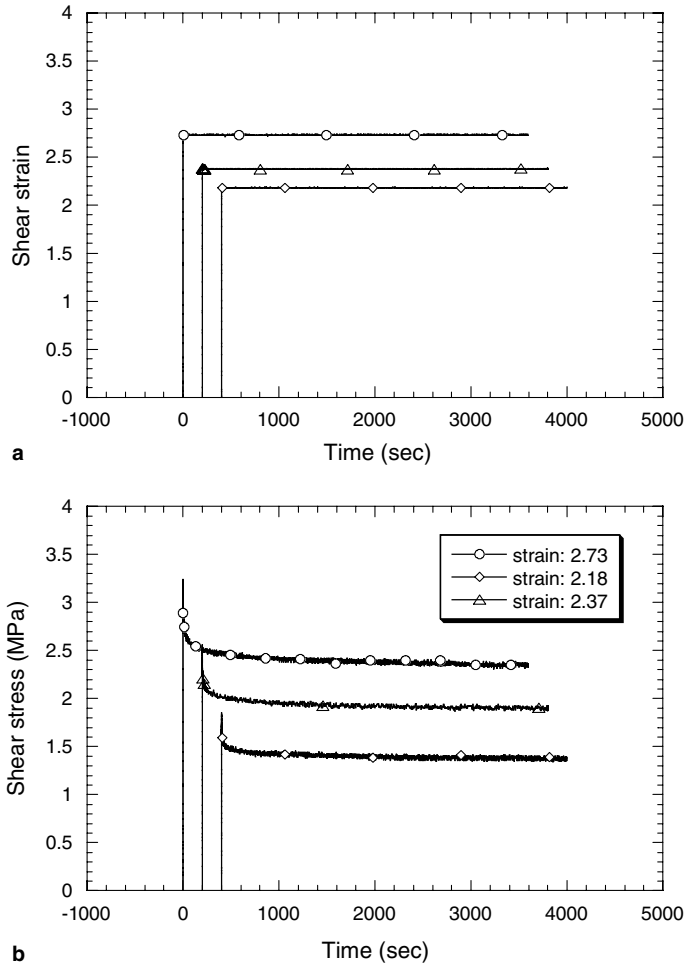

Fig. 7. Simple relaxation tests conducted on NR at different strain levels in shear regime: (a) applied strain history; (b) stress history. For the purpose of understandable illustration, the strain and stress histories have been separated from each other by 100 s. Stress and strain measures are further illustrated in Fig. 13.

a strain rate of 0.5/s was applied during the loading path while for the shear tests, the corresponding strain rate was 3.6/s. The stress relaxation was recorded for 600 s in the compression tests and for 3600 s in the shear tests.

Figs. 4(b) and 5(b) show the time histories of stress at different strain levels in compression and shear regimes in HDR obtained from simple relaxation tests. All curves reveal the existence of a very fast stress relaxation during the first 200 s followed by a very slow rate of relaxation that continues in an asymptotic sense. This conforms with observations reported by Haupt and Sedlan (2001). In the classical approach, equilibrium states are reached if the duration of the relaxation periods is infinitely long. Thus, the stresses measured at the termination points of the relaxation periods are approximate values of the equilibrium stress. The difference between the current stress and the equilibrium stress is the so-called overstress. Figs. 6(b) and 7(b) present the corresponding results obtained

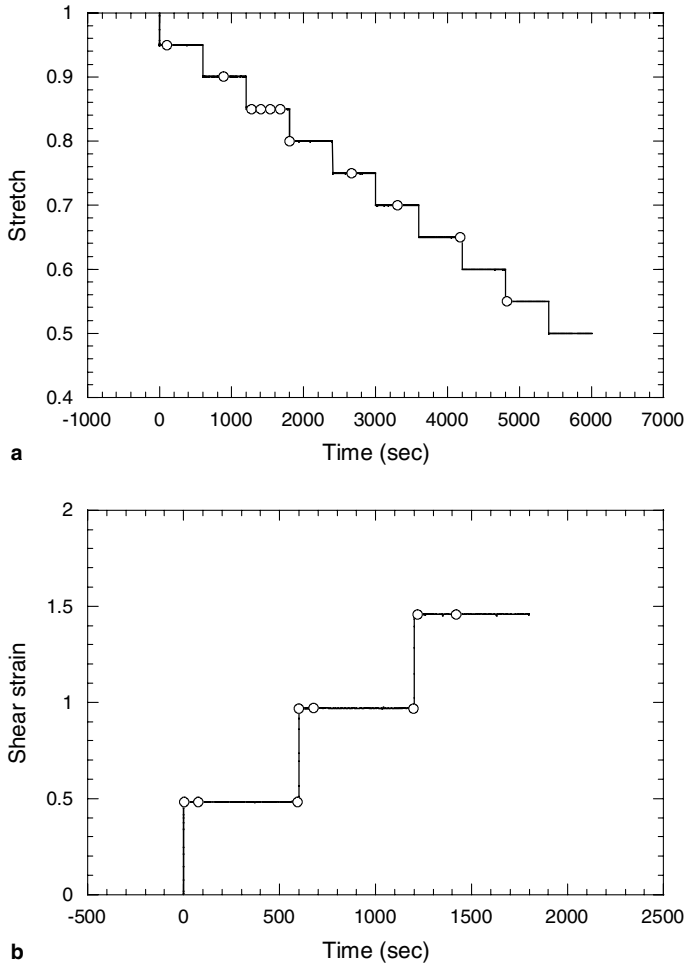

Fig. 8. Applied strain (stretch) histories in multi-step relaxation tests: (a) compression; (b) simple shear. Stress and strain measures are further illustrated in Fig. 13.

from NR where the overstresses are much lower than those observed in HDR at all strain levels. Comparing the results obtained at different strain levels, it can be seen that relaxation tests conducted on NR and HDR at higher strain levels possess larger overstresses and subsequently show a faster stress relaxation than those at lower strain levels with lower overstresses. This observation is similar to earlier results obtained from Adiprene-L100 (Khan and Lopez-Pamies, 2002). All these observations may have a relation with process-dependent changes in the microstructure of the material involving breakage and recovery of weak bonds of both the filler and the rubber matrix. A specimen under a large overstress is more likely to lose the crosslink bonds of the rubber–filler matrix than that under a small overstress. Such a loss of crosslink bonds corresponds to a faster relaxation of overstress in the very beginning of the relaxation process. Similar phenomena can also be seen in the case of NR, but in a way weaker than that of HDR, perhaps due to the presence of a lower filler content. However, the very slow stress decay as observed in the range

of the long-term relaxation may arise from the relaxation of the rubber matrix itself and might have a little relation with the filler-rubber bonds that are already broken. Thus, the long term relaxation behavior of HDR and NR is found to be comparable. Such a notion also is conformed by the results of cyclic tests, which have shown a weak rate dependence during unloading (Figs. 2 and 3, Section 2.1). Such phenomena may be involved with the relaxation of rubber networks with broken rubber–filler bonds. Nevertheless, the stress relaxation phenomena observed in NR and HDR over the recorded time history were found to be continuous one suggesting a gradual change within the microstructure. All observations are important in the sense of developing an experimentally-based constitutive equation for the viscosity that will be introduced in Section 4.

The results obtained from simple relaxation tests presented in Figs. 4–7 have shown the asymptotic attainment of equilibrium states at the end of each relaxation process. This idea

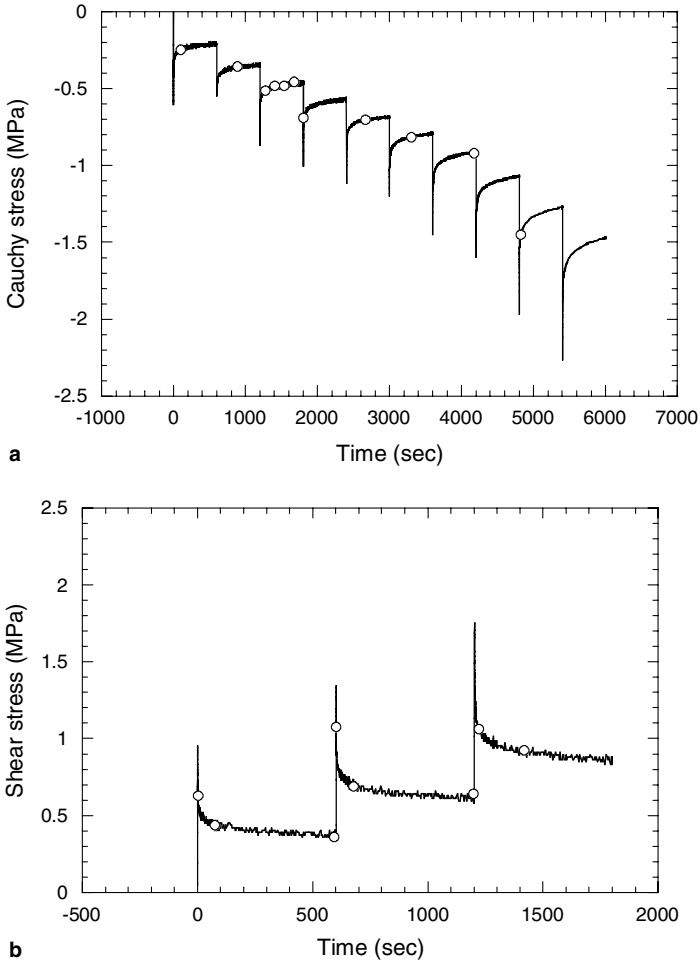

Fig. 9. Stress history recorded in multi-step relaxation tests on HDR: (a) compression; (b) simple shear. Stress and strain measures are further illustrated in Fig. 13.

was also explored by Lion (1996, 1997), Bergström and Boyce (1998) and Amin et al. (2002). It is followed to estimate the equilibrium response for the specimens in compression and shear deformations (see Amin et al., 2006) through multi-step relaxation tests. Figs. 8(a) and (b) show different strain histories as applied to compression and shear specimens. The time histories of relaxation obtained at each step are illustrated in Figs. 9 and 10 for HDR and NR specimens. The figures demonstrate the effect of 'overstress experienced just at the very beginning of the stress relaxation history' of a particular strain step on the relaxation phenomenon of that particular step. The results display a very fast relaxation rate just after a strain step, where the overstress is large. Thus, the role of 'overstress experienced just at the very beginning of relaxation history' comes out as a dominant factor in deciding the relaxation rate of a particular step. Such a quantity bears a direct relevance with the current strain state. Interested readers are referred to Sections 4 and 5 for further evaluation of these experimental observations as well as the subsequent discussion.

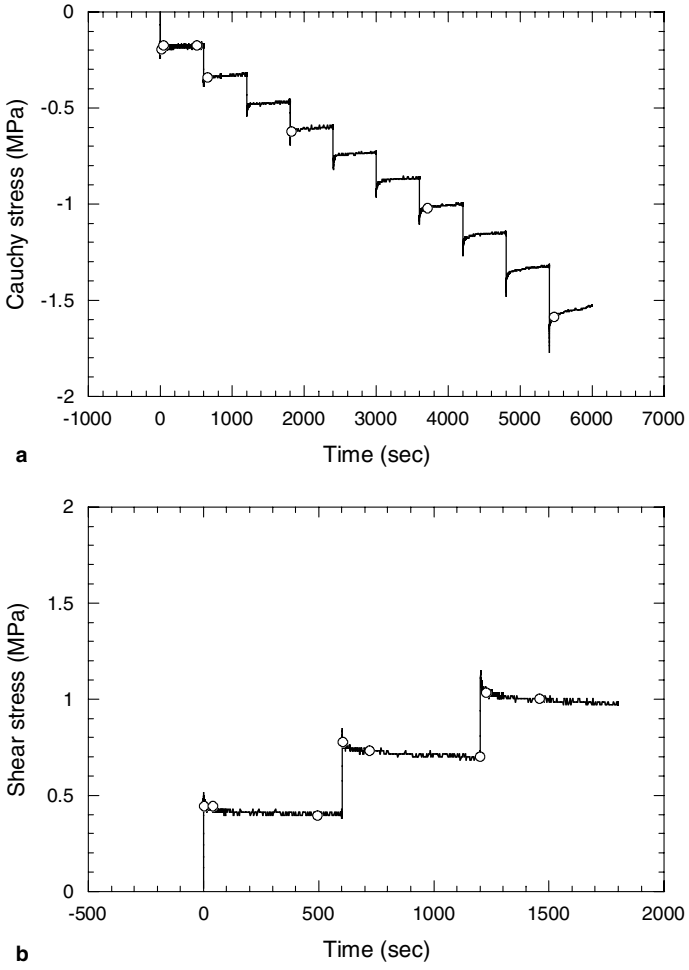

Fig. 10. Stress history recorded in multi-step relaxation tests on NR: (a) compression; (b) simple shear. Stress and strain measures are further illustrated in Fig. 13.

3. Constitutive model

The experimental observations presented in Section 2 illustrate rate-dependent phenomena in both HDR and NR. The phenomena observed under large strains suggest for a model of finite strain viscoelasticity as sketched in Fig. 1. This section introduces a model of this type that follows from the concept of Huber and Tsakmakis (2000a,b). It is based on the multiplicative decomposition of the deformation gradient and the additive split of the free energy as introduced by Lubliner (1985). The presentation leads to a discussion about different possibilities of incorporating appropriate process variables to arrive at a nonlinear evolution equation for the inelastic strain rate. Finally, an improved hyperelasticity model has been introduced for having adequate descriptions of the free energies.

In the finite strain kinematics, the local mapping between the initial and current configuration of a deformable body under motion is described by the deformation gradient tensor $\mathbf{F}$

$$\mathbf{F} = \sum_{\alpha=1}^{3} \lambda_\alpha \mathbf{n}_\alpha \otimes \mathbf{N}_\alpha, \tag{1}$$

where $\lambda_\alpha = 1 + \Delta L_\alpha / L_\alpha$ are the stretches in the three principal directions, L_α are the undeformed lengths of material line elements and ΔL_α their changes. $\mathbf{N}_\alpha$ and $\mathbf{n}_\alpha$ are the material and spatial vector triads. The left-Cauchy Green tensor $\mathbf{B}$ describes the deformation and I_B, II_B and III_B are the invariants of $\mathbf{B}$:

$$\mathbf{B} = \mathbf{F}\mathbf{F}^{\mathrm{T}} = \sum_{\alpha=1}^{3} \lambda_\alpha^2 \mathbf{n}_\alpha \otimes \mathbf{n}_\alpha, \tag{2}$$

$$I_B = \operatorname{tr}\mathbf{B}, \quad II_B = \frac{1}{2} = \{(\operatorname{tr}\mathbf{B})^2 - \operatorname{tr}(\mathbf{B}^2)\}, \quad III_B = \det\mathbf{B}. \tag{3}$$

The velocity gradient $\mathbf{L}$ and the deformation rate tensor $\mathbf{D}$ are defined as follows:

$$\mathbf{L} = \dot{\mathbf{F}}\mathbf{F}^{-1}, \tag{4}$$

$$\mathbf{D} = \frac{1}{2}(\mathbf{L} + \mathbf{L}^{\mathrm{T}}). \tag{5}$$

To represent rate-dependent material behavior, small strain theories are based on an additive decomposition of the total strain into elastic and inelastic parts denoted by $\mathbf{e}_{\mathrm{e}}$ and $\mathbf{e}_{\mathrm{i}}$ in Fig. 1. The corresponding relation in the theory of finite strains can be attained through the multiplicative decomposition of the deformation gradient $\mathbf{F}$ into an elastic part $\mathbf{F}_{\mathrm{e}}$ and an inelastic part $\mathbf{F}_{\mathrm{i}}$

$$\mathbf{F} = \mathbf{F}_{\mathrm{e}}\mathbf{F}_{\mathrm{i}}. \tag{6}$$

This decomposition introduces the so-called inelastic intermediate configuration as sketched in Fig. 11. It can be obtained, when the stress is removed with an infinitely fast rate to an equilibrium state keeping the value of $\mathbf{F}_{\mathrm{i}}$ constant during the unloading process. Since rubber has a fairly large compression modulus in comparison with its shear modulus, we assume the material to be incompressible in the following:

$$\det\mathbf{F} = \det\mathbf{F}_{\mathrm{e}} = \det\mathbf{F}_{\mathrm{i}} = 1. \tag{7}$$

Experimental observations presented in Amin et al. (2003) also substantiate this fact within the practical ranges for HDR and NR material.

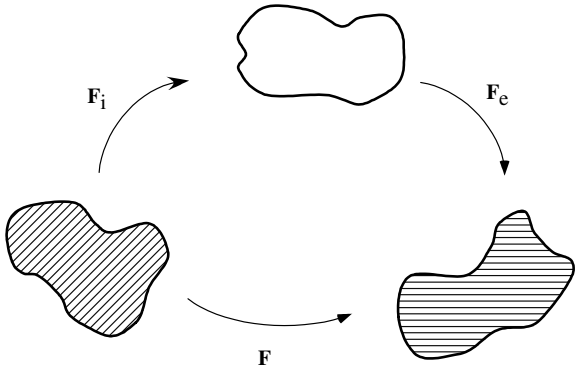

Fig. 11. Multiplicative decomposition of deformation gradient tensor, $\mathbf{F}$ into an elastic part $\mathbf{F}_e$ and an inelastic part $\mathbf{F}_i$.

As a consequence of the multiplicative split defined by Eq. (6), the left Cauchy Green tensors $\mathbf{B}_e$ and $\mathbf{B}_i$ associated with elastic and inelastic deformations are defined as follows:

$$\mathbf{B}_e = \mathbf{F}_e\mathbf{F}_e^T, \quad \mathbf{B}_i = \mathbf{F}_i\mathbf{F}_i^T. \tag{8}$$

Calculating the material time rate $\dot{\mathbf{B}}_e = \dot{\mathbf{F}}_e\mathbf{F}_e^T + \mathbf{F}_e\dot{\mathbf{F}}_e^T$ and replacing the rate of the elastic part of deformation gradient using $\dot{\mathbf{F}}_e = \mathrm{d}/\mathrm{d}t(\mathbf{F}\mathbf{F}_i^{-1}) = \mathbf{L}\mathbf{F}_e - \mathbf{F}_e\hat{\mathbf{L}}_i$, we obtain

$$\dot{\mathbf{B}}_e = -2\mathbf{F}_e\hat{\mathbf{D}}_i\mathbf{F}_e^T + \mathbf{B}_e\mathbf{L}^T + \mathbf{L}\mathbf{B}_e. \tag{9}$$

The inelastic velocity gradient $\hat{\mathbf{L}}_i$ and its symmetric part $\hat{\mathbf{D}}_i$ are defined as follows:

$$\hat{\mathbf{L}}_i = \dot{\mathbf{F}}_i\mathbf{F}_i^{-1}, \tag{10}$$

$$\hat{\mathbf{D}}_i = \frac{1}{2}(\hat{\mathbf{L}}_i + \hat{\mathbf{L}}_i^T). \tag{11}$$

Since $\det\mathbf{F} = 1$ is valid for incompressible materials, the weighted Cauchy stress $\mathbf{S} = (\det\mathbf{F})\mathbf{T}$ is equal to the Cauchy stress, i.e., $\mathbf{S} = \mathbf{T}$. The incompressibility constraint also implies an additive constitutively non-determined contribution "$-p\mathbf{1}$" to the stress. As a result, we have

$$\mathbf{S} = -p\mathbf{1} + \mathbf{S}_E, \tag{12}$$

where p is the hydrostatic pressure which needs to be determined from the boundary conditions of the problem under consideration. Following the idea of the Zener model, the extra stress $\mathbf{S}_E$ is the sum of a rate-independent equilibrium stress $\mathbf{S}_E^{(E)}$ and a rate-dependent overstress $\mathbf{S}_E^{(OE)}$ (cf. Fig. 12)

$$\mathbf{S}_E = \mathbf{S}_E^{(E)} + \mathbf{S}_E^{(OE)}. \tag{13}$$

To formulate the constitutive relations for the two components of $\mathbf{S}_E$ it is common practice to evaluate the isothermal form of Clausius Duhem inequality (Coleman and Gurtin, 1967)

$$-\rho_R\dot{\Psi} + \mathbf{S}_E \cdot \mathbf{L} \geqslant 0. \tag{14}$$

Due to $\det\mathbf{F} = 1$, or equivalently $\mathrm{tr}\,\mathbf{L} = 0$, the power of the constraint stress and the geometric compatible motions $(-p\mathbf{1}) \cdot \mathbf{L}$ is zero and does not occur in Eq. (14). ρ_R is the mass

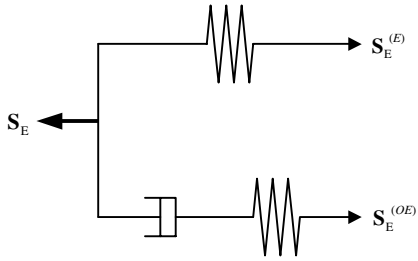

Fig. 12. Decomposition of stress in Zener model.

density of the material in the reference configuration and Ψ the Helmholtz free energy per unit mass.

For the material under consideration, an additive split of the free energy into the sum of an equilibrium part $w^{(\mathrm{E})}$ and non-equilibrium part $w^{(\mathrm{OE})}$ is proposed

$$\rho_{\mathrm{R}}\Psi = w^{(\mathrm{E})}(I_B, II_B) + w^{(\mathrm{OE})}(I_{B_\mathrm{e}}, II_{B_\mathrm{e}}). \tag{15}$$

Since the material is assumed to be incompressible and isotropic, the contributions of the free energy depend only on the first and second invariants of $\mathbf{B}$ and $\mathbf{B}_\mathrm{e}$ as defined in Eq. (3). As a consequence of the assumption of isotropy the corresponding stresses $\mathbf{S}_{\mathrm{E}}^{(\mathrm{E})} = \mathbf{f}(\mathbf{B})$ and $\mathbf{S}_{\mathrm{E}}^{(\mathrm{OE})} = \mathbf{g}(\mathbf{B}_\mathrm{e})$ are isotropic tensor functions of their arguments $\mathbf{B}$ and $\mathbf{B}_\mathrm{e}$. This leads to the following interchangeability relations:

$$\mathbf{B}\mathbf{S}_{\mathrm{E}}^{(\mathrm{E})} = \mathbf{S}_{\mathrm{E}}^{(\mathrm{E})}\mathbf{B}, \quad \mathbf{B}_\mathrm{e}\mathbf{S}_{\mathrm{E}}^{(\mathrm{OE})} = \mathbf{S}_{\mathrm{E}}^{(\mathrm{OE})}\mathbf{B}_\mathrm{e}. \tag{16}$$

Representation formulae of isotropic tensor functions are derived in Haupt (2000). For the time rate of the free energy the expression

$$\rho_{\mathrm{R}}\dot{\Psi} = \frac{\partial w^{(\mathrm{E})}}{\partial I_B}\dot{I}_B + \frac{\partial w^{(\mathrm{E})}}{\partial II_B}\dot{II}_B + \frac{\partial w^{(\mathrm{OE})}}{\partial I_{B_\mathrm{e}}}\dot{I}_{B_\mathrm{e}} + \frac{\partial w^{(\mathrm{OE})}}{\partial II_{B_\mathrm{e}}}\dot{II}_{B_\mathrm{e}} \tag{17a}$$

is calculated. Considering

$$\dot{I}_B = \mathbf{1}\cdot\dot{\mathbf{B}}, \quad \dot{II}_B = (I_B\mathbf{1} - \mathbf{B})\cdot\dot{\mathbf{B}}, \quad \dot{I}_{B_\mathrm{e}} = \mathbf{1}\cdot\dot{\mathbf{B}}_\mathrm{e}, \quad \dot{II}_{B_\mathrm{e}} = (I_{B_\mathrm{e}}\mathbf{1} - \mathbf{B}_\mathrm{e})\cdot\dot{\mathbf{B}}_\mathrm{e} \tag{17b}$$

for the time rates of the strain invariants and taking the Cayley–Hamilton equation in the form of $\mathbf{B} = I_B\mathbf{1} - II_B\mathbf{B}^{-1} + III_B\mathbf{B}^{-2}$ and $\mathbf{B}_\mathrm{e} = I_{B_\mathrm{e}}\mathbf{1} - II_{B_\mathrm{e}}\mathbf{B}_\mathrm{e}^{-1} + III_{B_\mathrm{e}}\mathbf{B}_\mathrm{e}^{-2}$ into account (see, e.g., Haupt, 2000), Eq. (17a) can also be written in the following form:

$$\begin{aligned}\rho_{\mathrm{R}}\dot{\Psi} = &\left\{\frac{\partial w^{(\mathrm{E})}}{\partial I_B}\mathbf{1} + \frac{\partial w^{(\mathrm{E})}}{\partial II_B}(II_B\mathbf{B}^{-1} - \mathbf{B}^{-2})\right\}\cdot\dot{\mathbf{B}} \\ &+ \left\{\frac{\partial w^{(\mathrm{OE})}}{\partial I_{B_\mathrm{e}}}\mathbf{1} + \frac{\partial w^{(\mathrm{OE})}}{\partial II_{B_\mathrm{e}}}(II_B\mathbf{B}_\mathrm{e}^{-1} - \mathbf{B}_\mathrm{e}^{-2})\right\}\cdot\dot{\mathbf{B}}_\mathrm{e}.\end{aligned} \tag{17c}$$

Since the rate of the free energy is proportional to the time rates of the Cauchy Green tensors $\mathbf{B}$ and $\mathbf{B}_\mathrm{e}$ the stress power is reformulated in the following. Considering Eqs. (4) and (6) the velocity gradient decomposes into the sum of a pure elastic and a mixed part

$$\mathbf{L} = \dot{\mathbf{F}}_\mathrm{e}\mathbf{F}_\mathrm{e}^{-1} + \mathbf{F}_\mathrm{e}\dot{\mathbf{F}}_\mathrm{i}\mathbf{F}_\mathrm{i}^{-1}\mathbf{F}_\mathrm{e}^{-1} = \mathbf{L}_\mathrm{e} + \mathbf{F}_\mathrm{e}\hat{\mathbf{L}}_\mathrm{i}\mathbf{F}_\mathrm{e}^{-1}. \tag{18}$$

Taking Eq. (13) into account, the stress power splits into the power of the equilibrium stress and the power of the overstress with respect to elastic and inelastic deformations

$$\mathbf{S}_{\mathrm{E}} \cdot \mathbf{L} = \mathbf{S}_{\mathrm{E}}^{(\mathrm{E})} \cdot \mathbf{L} + \mathbf{S}_{\mathrm{E}}^{(\mathrm{OE})} \cdot \mathbf{L}_{\mathrm{e}} + (\mathbf{F}_{\mathrm{e}}^{-1}\mathbf{S}_{\mathrm{E}}^{(\mathrm{OE})}\mathbf{F}_{\mathrm{e}}) \cdot \hat{\mathbf{L}}_{\mathrm{i}}^{\mathrm{T}}. \tag{19}$$

Since the isotropic tensor function $\mathbf{S}_{\mathrm{E}}^{(\mathrm{OE})} = \mathbf{g}(\mathbf{B}_{\mathrm{e}})$ depends only on integer powers of $\mathbf{B}_{\mathrm{e}}$, the stress tensor $\mathbf{F}_{\mathrm{e}}^{-1}\mathbf{S}_{\mathrm{E}}^{(\mathrm{OE})}\mathbf{F}_{\mathrm{e}} = \mathbf{g}(\mathbf{C}_{\mathrm{e}})$ is also symmetric. This becomes clear when calculating $\mathbf{F}_{\mathrm{e}}^{-1}(\mathbf{B}_{\mathrm{e}})^{n}\mathbf{F}_{\mathrm{e}} = (\mathbf{C}_{\mathrm{e}})^{n}$, where n is an arbitrary integer number and $\mathbf{C}_{\mathrm{e}} = \mathbf{F}_{\mathrm{e}}^{\mathrm{T}}\mathbf{F}_{\mathrm{e}}$ is the right Cauchy Green tensor. Thus, the inelastic velocity gradient in Eq. (19) can be replaced by its symmetric part

$$\mathbf{S}_{\mathrm{E}} \cdot \mathbf{L} = \mathbf{S}_{\mathrm{E}}^{(\mathrm{E})} \cdot \mathbf{L} + \mathbf{S}_{\mathrm{E}}^{(\mathrm{OE})} \cdot \mathbf{L}_{\mathrm{e}} + (\mathbf{F}_{\mathrm{e}}^{-1}\mathbf{S}_{\mathrm{E}}^{(\mathrm{OE})}\mathbf{F}_{\mathrm{e}}) \cdot \hat{\mathbf{D}}_{\mathrm{i}}. \tag{20}$$

Calculating the time rates $\dot{\mathbf{B}} = \mathrm{d}/\mathrm{d}t(\mathbf{F}\mathbf{F}^{\mathrm{T}}) = \mathbf{L}\mathbf{B} + \mathbf{B}\mathbf{L}^{\mathrm{T}}$ and $\dot{\mathbf{B}}_{\mathrm{e}} = \mathrm{d}/\mathrm{d}t(\mathbf{F}_{\mathrm{e}}\mathbf{F}_{\mathrm{e}}^{\mathrm{T}}) = \mathbf{L}_{\mathrm{e}}\mathbf{B}_{\mathrm{e}} + \mathbf{B}_{\mathrm{e}}\mathbf{L}_{\mathrm{e}}^{\mathrm{T}}$ the total and elastic velocity gradients can be expressed as

$$\mathbf{L} = \dot{\mathbf{B}}\mathbf{B}^{-1} - \mathbf{B}\mathbf{L}^{\mathrm{T}}\mathbf{B}^{-1} \quad \text{and} \quad \mathbf{L}_{\mathrm{e}} = \dot{\mathbf{B}}_{\mathrm{e}}\mathbf{B}_{\mathrm{e}}^{-1} - \mathbf{B}_{\mathrm{e}}\mathbf{L}_{\mathrm{e}}^{\mathrm{T}}\mathbf{B}_{\mathrm{e}}^{-1}. \tag{21}$$

Considering that $\mathbf{S}_{\mathrm{E}}^{(\mathrm{E})} = \mathbf{f}(\mathbf{B})$ is an isotropic function of $\mathbf{B}$, i.e., $\mathbf{B}^{-1}\mathbf{S}_{\mathrm{E}}^{(\mathrm{E})}\mathbf{B} = \mathbf{S}_{\mathrm{E}}^{(\mathrm{E})}$, the first term on the right-hand side of Eq. (20) can be reformulated as

$$\begin{aligned}\mathbf{S}_{\mathrm{E}}^{(\mathrm{E})} \cdot \mathbf{L} &= \mathrm{tr}(\mathbf{S}_{\mathrm{E}}^{(\mathrm{E})}\dot{\mathbf{B}}\mathbf{B}^{-1} - \mathbf{S}_{\mathrm{E}}^{(\mathrm{E})}\mathbf{B}\mathbf{L}^{\mathrm{T}}\mathbf{B}^{-1}) = \mathrm{tr}(\mathbf{B}^{-1}\mathbf{S}_{\mathrm{E}}^{(\mathrm{E})}\dot{\mathbf{B}} - \mathbf{B}^{-1}\mathbf{S}_{\mathrm{E}}^{(\mathrm{E})}\mathbf{B}\mathbf{L}^{\mathrm{T}}) \\ &= (\mathbf{B}^{-1}\mathbf{S}_{\mathrm{E}}^{(\mathrm{E})}) \cdot \dot{\mathbf{B}} - \mathbf{S}_{\mathrm{E}}^{(\mathrm{E})} \cdot \mathbf{L}\end{aligned}$$

leading finally to

$$\mathbf{S}_{\mathrm{E}}^{(\mathrm{E})} \cdot \mathbf{L} = \frac{1}{2}(\mathbf{B}^{-1}\mathbf{S}_{\mathrm{E}}^{(\mathrm{E})}) \cdot \dot{\mathbf{B}}. \tag{22}$$

A similar argumentation leads to the expression

$$\mathbf{S}_{\mathrm{E}}^{(\mathrm{OE})} \cdot \mathbf{L}_{\mathrm{e}} = \frac{1}{2}(\mathbf{B}_{\mathrm{e}}^{-1}\mathbf{S}_{\mathrm{E}}^{(\mathrm{OE})}) \cdot \dot{\mathbf{B}}_{\mathrm{e}} \tag{23}$$

for the elastic power of the overstress. Inserting Eqs. (22) and (23) into Eq. (20) we obtain

$$\mathbf{S}_{\mathrm{E}} \cdot \mathbf{L} = \frac{1}{2}(\mathbf{B}^{-1}\mathbf{S}_{\mathrm{E}}^{(\mathrm{E})}) \cdot \dot{\mathbf{B}} + \frac{1}{2}(\mathbf{B}_{\mathrm{e}}^{-1}\mathbf{S}_{\mathrm{E}}^{(\mathrm{OE})}) \cdot \dot{\mathbf{B}}_{\mathrm{e}} + (\mathbf{F}_{\mathrm{e}}^{-1}\mathbf{S}_{\mathrm{E}}^{(\mathrm{OE})}\mathbf{F}_{\mathrm{e}}) \cdot \hat{\mathbf{D}}_{\mathrm{i}}, \tag{24}$$

i.e., the stress power contains two terms which are proportional to the time rates of the total and the elastic left Cauchy Green tensors. Inserting Eqs. (19) and (24) into the Clausius Duhem inequality, Eq. (14), and rearranging terms leads to

$$\begin{aligned}&\left\{\frac{1}{2}(\mathbf{B}^{-1}\mathbf{S}_{\mathrm{E}}^{(\mathrm{E})}) - \left(\frac{\partial w^{(\mathrm{E})}}{\partial I_B}\mathbf{1} + \frac{\partial w^{(\mathrm{E})}}{\partial II_B}(I_B\mathbf{B}^{-1} - \mathbf{B}^{-2})\right)\right\} \cdot \dot{\mathbf{B}} + (\mathbf{F}_{\mathrm{e}}^{-1}\mathbf{S}_{\mathrm{E}}^{(\mathrm{OE})}\mathbf{F}_{\mathrm{e}}) \cdot \hat{\mathbf{D}}_{\mathrm{i}} \\ &\quad + \left\{\frac{1}{2}(\mathbf{B}_{\mathrm{e}}^{-1}\mathbf{S}_{\mathrm{E}}^{(\mathrm{OE})}) - \left(\frac{\partial w^{(\mathrm{OE})}}{\partial I_{B_{\mathrm{e}}}}\mathbf{1} + \frac{\partial w^{(\mathrm{OE})}}{\partial II_{B_{\mathrm{e}}}}(I_B\mathbf{B}_{\mathrm{e}}^{-1} - \mathbf{B}_{\mathrm{e}}^{-2})\right)\right\} \cdot \dot{\mathbf{B}}_{\mathrm{e}} \geqslant 0,\end{aligned} \tag{25}$$

which has to be satisfied for arbitrary processes. Since $\mathbf{B}$ and $\mathbf{B}_{\mathrm{e}}$ are the independent variables of the free energy their rates can be varied, in principle, arbitrarily. In order to satisfy Eq. (25) the corresponding factors of proportionality have to vanish which leads to the following stress–strain relations:

$$\mathbf{S}_{\mathrm{E}}^{(\mathrm{E})} = 2\frac{\partial w^{(\mathrm{E})}}{\partial I_B}\mathbf{B} + 2\frac{\partial w^{(\mathrm{E})}}{\partial II_B}(I_B\mathbf{1} - \mathbf{B}^{-1}), \tag{26}$$

$$\mathbf{S}_{\mathrm{E}}^{(\mathrm{OE})} = 2\frac{\partial w^{(\mathrm{OE})}}{\partial I_{B_{\mathrm{e}}}}\mathbf{B}_{\mathrm{e}} + 2\frac{\partial w^{(\mathrm{OE})}}{\partial II_{B_{\mathrm{e}}}}(I_B\mathbf{1} - \mathbf{B}_{\mathrm{e}}^{-1}). \tag{27}$$

Since the hydrostatic pressure in Eq. (12), $\mathbf{S} = -p\mathbf{1} + S_{\mathrm{E}}$, is constitutively undetermined, the terms which are proportional to the unit tensor in Eqs. (26) and (27) can be omitted:

$$\mathbf{S}_{\mathrm{E}}^{(\mathrm{E})} = 2\frac{\partial w^{(\mathrm{E})}}{\partial I_B}\mathbf{B} - 2\frac{\partial w^{(\mathrm{E})}}{\partial II_B}\mathbf{B}^{-1}, \tag{28}$$

$$\mathbf{S}_{\mathrm{E}}^{(\mathrm{OE})} = 2\frac{\partial w^{(\mathrm{OE})}}{\partial I_{B_{\mathrm{e}}}}\mathbf{B}_{\mathrm{e}} - 2\frac{\partial w^{(\mathrm{OE})}}{\partial II_{B_{\mathrm{e}}}}\mathbf{B}_{\mathrm{e}}^{-1}. \tag{29}$$

To represent the behavior of rubber, the strain energies $w^{(\mathrm{E})}$ and $w^{(\mathrm{OE})}$ have to be adequate to represent both the equilibrium and instantaneous responses of the material.

To specify the constitutive equation describing the temporal evolution of the inelastic strains the so-called residual inequality following from Eqs. (25)–(27) is considered

$$(\mathbf{F}_{\mathrm{e}}^{-1}\mathbf{S}_{\mathrm{E}}^{(\mathrm{OE})}\mathbf{F}_{\mathrm{e}}) \cdot \hat{\mathbf{D}}_{\mathrm{i}} \geqslant 0. \tag{30}$$

It expresses that the power between the overstress and the inelastic strain rate has to be non-negative. The most simple flow rule satisfying Eq. (30) for arbitrary processes reads as

$$\hat{\mathbf{D}}_{\mathrm{i}} = \frac{1}{\eta}\mathbf{F}_{\mathrm{e}}^{-1}\mathbf{S}_{\mathrm{E}}^{(\mathrm{OE})}\mathbf{F}_{\mathrm{e}}, \quad \eta(\ldots) > 0, \tag{31}$$

where the viscosity η can be, in principle, an arbitrary positive functional of the process history. For example, a stress-dependent viscosity function would correspond to nonlinear rate-dependent material responses. Since the material under discussion is incompressible, we have $\operatorname{tr}\hat{\mathbf{L}}_{\mathrm{i}} = \operatorname{tr}\hat{\mathbf{D}}_{\mathrm{i}} = 0$ and thus a deviatoric tensor $\hat{\mathbf{D}}_{\mathrm{i}}$. Taking $\mathbf{F}_{\mathrm{e}}^{-1}(\mathbf{B}_{\mathrm{e}})^n\mathbf{F}_{\mathrm{e}} = (\mathbf{C}_{\mathrm{e}})^n$ where n is an arbitrary integer number into account and considering $I_{C_{\mathrm{e}}} = I_{B_{\mathrm{e}}}$ and $II_{C_{\mathrm{e}}} = II_{B_{\mathrm{e}}}$, Eq. (29) leads to the stress tensor

$$\mathbf{F}_{\mathrm{e}}^{-1}\mathbf{S}_{\mathrm{E}}^{(\mathrm{OE})}\mathbf{F}_{\mathrm{e}} = 2\frac{\partial w^{(\mathrm{OE})}}{\partial I_{C_{\mathrm{e}}}}\mathbf{C}_{\mathrm{e}} - 2\frac{\partial w^{(\mathrm{OE})}}{\partial II_{C_{\mathrm{e}}}}\mathbf{C}_{\mathrm{e}}^{-1}. \tag{32}$$

With the definition of the overstress tensor

$$\hat{\boldsymbol{\tau}}_{\mathrm{E}}^{(\mathrm{OE})} = \mathbf{F}_{\mathrm{e}}^{-1}\mathbf{S}_{\mathrm{E}}^{(\mathrm{OE})}\mathbf{F}_{\mathrm{e}}^{T-1} \tag{33}$$

operating on the inelastic intermediate configuration, the relation

$$\mathbf{F}_{\mathrm{e}}^{-1}\mathbf{S}_{\mathrm{E}}^{(\mathrm{OE})}\mathbf{F}_{\mathrm{e}} = \mathbf{C}_{\mathrm{e}}\hat{\boldsymbol{\tau}}_{\mathrm{E}}^{(\mathrm{OE})} = \hat{\mathbf{P}}_{\mathrm{E}}^{(\mathrm{OE})} \tag{34}$$

is obtained, where $\hat{\mathbf{P}}_{\mathrm{E}}^{(\mathrm{OE})}$ is the so-called Mandel stress tensor (cf. Huber and Tsakmakis, 2000a,b or Lubliner, 1986). Since $\hat{\mathbf{D}}_{\mathrm{i}}$ is a deviator, Eq. (31) can be written as follows:

$$\hat{\mathbf{D}}_{\mathrm{i}} = \frac{1}{\eta(\ldots)}(\hat{\mathbf{P}}_{\mathrm{E}} - \hat{\mathbf{P}}_{\mathrm{E}}^{(\mathrm{E})})^D. \tag{35}$$

In order to represent rate-dependent behavior for particular materials, it is necessary to express the viscosity as a function of process variables like deformation or overstress or as a function of internal variables (cf. Haupt, 2000). A dependence of the viscosity on an internal variable with its own time scale leads to thixotropic material behavior. Nevertheless, the choice of the internal variables and the formulation of an evolution equation in the three-dimensional form should ideally depend on the evaluation of test data obtained from experiments with real materials.

Furthermore, the model of finite strain viscoelasticity as presented here consists of nonlinear springs in two parallel branches to describe the equilibrium and instantaneous responses that correspond to infinitely slow and fast rates of deformation. These are rate-independent elastic responses that bound a domain where viscosity effects come into play (Huber and Tsakmakis, 2000a). An adequate description of their corresponding free energy functions $w^{(\mathrm{E})}(I_B,II_B)$ or $w^{(\mathrm{OE})}(I_{B_\mathrm{e}},II_{B_\mathrm{e}})$ is conventionally attained through hyperelasticity models to represent these boundary states. Such a description is essential for a physically meaningful representation of viscosity phenomena that occur within the so-called viscosity domain. However, due to the strong dependence of the stress on the state of strain, experiments are required to identify an adequate form of $w^{(\mathrm{E})}(I_B,II_B)$ or $w^{(\mathrm{OE})}(I_{B_\mathrm{e}},II_{B_\mathrm{e}})$. Ideally, such a function should have the capability to represent the stress responses at all possible deformation modes. In this context, the hyperelasticity model formulated on the basis of experimental observations on HDR and NR under compression and shear (see Amin et al., 2002, 2006) is adopted in the current work to describe the elastic responses. Eqs. (36) and (37) show the hyperelasticity relation for both the equilibrium and the overstress response, respectively:

$$w^{(\mathrm{E})}(I_B,II_B) = C_5^{(\mathrm{E})}(I_B-3)+\frac{C_3^{(\mathrm{E})}}{N+1}(I_B-3)^{N+1} + \frac{C_4^{(\mathrm{E})}}{M+1}(I_B-3)^{M+1}+C_2^{(\mathrm{E})}(II_B-3), \tag{36}$$

$$w^{(\mathrm{OE})}(I_{B_\mathrm{e}},II_{B_\mathrm{e}}) = C_5^{(\mathrm{OE})}(I_{B_\mathrm{e}}-3)+\frac{C_3^{(\mathrm{OE})}}{N+1}(I_{B_\mathrm{e}}-3)^{N+1} + \frac{C_4^{(\mathrm{OE})}}{M+1}(I_{B_\mathrm{e}}-3)^{M+1}+C_2^{(\mathrm{OE})}(II_{B_\mathrm{e}}-3), \tag{37}$$

where $C_5^{(\mathrm{E})}$, $C_3^{(\mathrm{E})}$, $C_4^{(\mathrm{E})}$, $C_2^{(\mathrm{E})}$, M and N are the material constants of the equilibrium relation while $C_5^{(\mathrm{E})}$, $C_3^{(\mathrm{E})}$, $C_4^{(\mathrm{E})}$, $C_2^{(\mathrm{E})}$ are those of the overstress. The incorporation of Eqs. (36) and (37) into Eqs. 28,29,31 and (35) leads to a thermodynamically consistent finite strain viscoelasticity model.

4. Experimental identification of the evolution of viscosity

In the preceding section, a general constitutive theory based on recent publications by Huber and Tsakmakis (2000a,b) has been introduced. In this formulation, the constitutive relation expressing the temporal evolution of the inelastic strain rate $\hat{\mathbf{D}}_\mathrm{i}$, the overstress tensor of the Mandel type $\hat{\mathbf{P}}_\mathrm{E}^{(\mathrm{OE})}$ is the driving force. The viscosity η serves as a factor of proportionality and may be assumed to be constant in the formulation of the simplest type. However, from experience of the authors, we believe that rate-dependent models with constant viscosities cannot represent the experimentally observed rate-dependent phenomena of rubber (Amin et al., 2002). Since the second law of thermodynamics only requires $\eta(\ldots)>0$ (Section 3), there is the possibility to generalize the flow rule and to introduce a dependence of the viscosity, for example, on stress, deformation or internal variables. To this end, the earlier concepts available in Reese and Govindjee (1998), Holzapfel (1996), Miehe and Keck (2000), and Haupt and Sedlan (2001) can be referred to, where different expressions were assumed to describe the nonlinear evolution of viscosity. In contrast to these efforts, the contribution of the current

work is to present a scheme to resolve viscosity phenomena by analyzing the experimental data and thereby achieving an adequate description of the evolution equation (Eq. (35)). The quest for having a physical understanding of the phenomena and their description through the evolution equation played as a major motivation for undertaking such an effort. Thus, the experimentally observed stress and strain histories belonging to relaxation tests under compression and shear have been used to calculate the fundamental $\hat{\mathbf{D}}_i$ vs. $\hat{\mathbf{P}}_E^{(OE)}$ relation for one-dimensional cases. On this basis, the dependence of different internal variables on this relation have been assessed to arrive at the constitutive equation for the viscosity that holds for both NR and HDR within the considered deformation ranges.

4.1. Scheme for analyzing stress relaxation data

A scheme is proposed to analyze the relaxation histories obtained from the experiments shown in Section 2 with the aim to calculate fundamental quantities of the Zener model, e.g., the rate of inelastic strain and the overstress associated with the Maxwell element connected in parallel with a spring (Fig. 1). The analysis is founded on the multiplicative decomposition of the deformation gradient $\mathbf{F}$ (Eq. (6), Fig. 11) into elastic $\mathbf{F}_e$ and inelastic $\mathbf{F}_i$ parts. Since the material is assumed to be isotropic and incompressible (Eq. (7)) the procedure presented here conforms with the constitutive model presented in Section 3. Yet, to utilize the experimental results the finite strain model needs to be degenerated into the corresponding one-dimensional form in accordance with the deformations applied in the experiments, e.g., uniaxial compression and simple shear.

If a specimen is subjected to uniaxial homogeneous compression (Section 2), the principal stretch λ_1 in the loading direction becomes compressed (Fig. 13(a)) and those in the two other directions λ_2 and λ_3 are under tension. Thus, the deformation gradient $\mathbf{F}$ reads as:

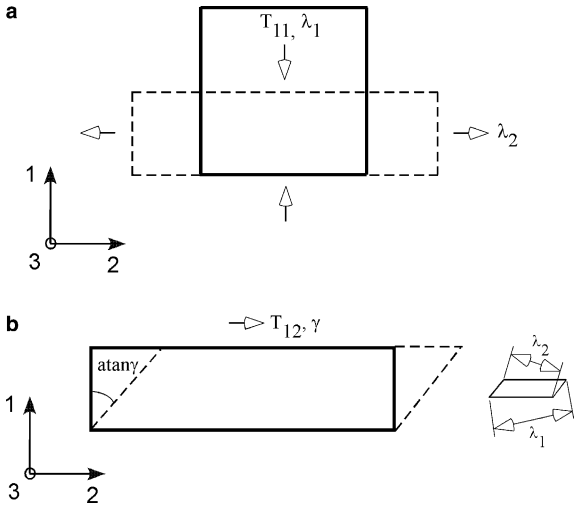

Fig. 13. Fundamental description of deformation: (a) homogeneous uniaxial compression; (b) simple shear.

$$\mathbf{F} = \begin{pmatrix} \lambda_1 & 0 & 0 \\ 0 & \lambda_2 & 0 \\ 0 & 0 & \lambda_3 \end{pmatrix}. \tag{38}$$

Considering isotropy and incompressibility we have $\lambda_2^2 = \lambda_3^2 = \lambda_1^{-1}$, while Eq. (3) leads the strain invariants to be

$$I = \frac{2}{\lambda_1} + \lambda_1^2, \quad II = \frac{1}{\lambda_1^2} + 2\lambda_1, \quad III = 1. \tag{39}$$

Since the lateral boundaries of the specimen are stress-free the weighted Cauchy stress tensor $\mathbf{S}$ is given by

$$\mathbf{S} = \begin{pmatrix} S_{11} & 0 & 0 \\ 0 & 0 & 0 \\ 0 & 0 & 0 \end{pmatrix}. \tag{40}$$

Following the multiplicative decomposition of $\mathbf{F}$ and utilizing Eq. (11) we further have:

$$\lambda_{1_i} = \frac{\lambda_1}{\lambda_{1_e}}, \tag{41}$$

$$D_{i_{11}} = \frac{\dot{\lambda}_{1_i}}{\lambda_{1_i}}, \tag{42}$$

where the subscripts i and e stand for inelastic and elastic parts of deformation. Furthermore, the extra part of the weighted Cauchy overstress $S_{11_E}^{(OE)}$ and the Mandel overstress, $P_{11_E}^{(OE)}$ become equal (Eq. (34)):

$$S_{11_E}^{(OE)} = P_{11_E}^{(OE)}. \tag{43}$$

Using Eqs. (29) and (37), the extra part of the overstress is obtained as

$$S_{11_E}^{(OE)} = 2\lambda_{1_e}^2 \left[C_5^{(OE)} + C_3^{(OE)} \left(\lambda_{1_e}^2 + \frac{2}{\lambda_{1_e}} - 3 \right)^N + C_4^{(OE)} \left(\lambda_{1_e}^2 + \frac{2}{\lambda_{1_e}} - 3 \right)^M \right] - \frac{2C_2^{(OE)}}{\lambda_{1_e}^2}, \tag{44}$$

where

$$S_{11_E}^{(OE)} = \frac{2}{3}(S_{11} - S_{11}^{(OE)}). \tag{45}$$

In order to establish a relation between theory and experiment, we note the equivalence of the experimentally recorded stresses as presented in Figs. 4 and 5 with the weighted Cauchy stress S_{11} (Eq. (45)), where material incompressibility is assumed (Eq. (7)). Furthermore, the values of the stress recorded at the termination points of the relaxation periods are regarded as equilibrium stresses, $S_{11}^{(E)}$. Based on this concept, it is possible to solve Eq. (44) along with (45) to calculate the elastic stretch λ_{1_e} for a particular value of $S_{11_E}^{(OE)}$. Due to the nonlinear form of Eq. (44), a numerical method may be applied to solve it. In the case of a simpler form of the hyperelasticity relation, for example a Neo-Hookean model, the solution procedure is simpler. Thus, the experimentally recorded relaxation history can be analyzed to obtain the time history of λ_{1_e}. The attainment of the time history of

D_{11_i} by taking the time derivatives over the experimental data points follows naturally from Eqs. (41) and (42).

The scheme presented by Eqs. (38)–(45) is applied for analyzing uniaxial compression data but it can also be formulated for simple shear. In this case, the direction of the applied displacement does not coincide with the directions of the principal stretches; rather it involves a rotation of axes (Fig. 13(b)). Due to the applied shear strain γ, the deformation gradient $\mathbf{F}$, its inelastic part $\mathbf{F}_i$ and the strain invariants are described as:

$$\mathbf{F} = \begin{pmatrix} 1 & \gamma & 0 \\ 0 & 1 & 0 \\ 0 & 0 & 1 \end{pmatrix}, \quad \mathbf{F}_i = \begin{pmatrix} 1 & \gamma_i & 0 \\ 0 & 1 & 0 \\ 0 & 0 & 1 \end{pmatrix}, \tag{46}$$

$$I = II = 3 + \gamma^2, \quad III = 1. \tag{47}$$

The equations corresponding to Eqs. (40)–(45) can also be written for simple shear as

$$\mathbf{S} = \begin{pmatrix} S_{11} & S_{12} & 0 \\ S_{12} & S_{22} & 0 \\ 0 & 0 & S_{33} \end{pmatrix}. \tag{48}$$

Calculating $\mathbf{F}_e = \mathbf{F}\mathbf{F}_i^{-1}$, the inelastic shear strain and its rate can be expressed as:

$$\gamma_i = \gamma - \gamma_e, \tag{49}$$

$$D_{i_{12}} = \dot{\gamma}_i. \tag{50}$$

The extra part of the stresses are written as:

$$S_{12_E}^{(OE)} = P_{12_E}^{(OE)}, \tag{51}$$

$$S_{12_E}^{(OE)} = 2\gamma_e \left[C_5^{(OE)} + C_2^{(OE)} + C_3^{(OE)} \gamma_e^{2N} + C_4^{(OE)} \gamma_e^{2M} \right], \tag{52}$$

where

$$S_{12_E}^{(OE)} = S_{12}^{(OE)} = S_{12} - S_{12}^{(E)}. \tag{53}$$

4.2. Evaluation of experimental results and proposal for an evolution equation

The evaluation scheme proposed in Section 4.1 has been used in this section to calculate the histories of D_{11_i}, D_{12_i}, $P_{11_E}^{(OE)}$ and $P_{12_E}^{(OE)}$ from the experimental data using Eqs. (42)–(45) and (49)–(53). In order to solve these relations, it is necessary to describe the overstress response adequately by Eqs. (44) and (52) through a set of material parameters that hold for both compression and shear. To this end, the set of material parameters for the equilibrium and instantaneous stress responses for HDR and NR obtained earlier (Amin et al., 2006) has been applied. The identification procedure has simultaneously minimized the least-square residuals of uniaxial compression and simple shear data. Table 1 presents the set of estimated parameters for HDR and NR. In this procedure, the multi-step relaxation data (Figs. 8–10) was used to trace the equilibrium curve. The instantaneous response was approximated from the asymptotic convergence (see Amin et al., 2002) of the loading phase response of the cyclic tests (Figs. 2 and 3) conducted at high strain rates. The parameters obtained for the equilibrium stress were subtracted from those of the

Table 1
Elasticity parameters for HDR and NR

Specimens	Responses	C_2 (MPa)	C_3 (MPa)	C_4 (MPa)	C_5 (MPa)	M	N
HDR	Equilibrium	0.145	1.182	−5.297	4.262	0.06	0.27
	Instantaneous	0.166	2.477	−11.689	9.707		
	Overstress	0.021	1.295	−6.392	5.445		
NR	Equilibrium	0.095	0.019	−0.515	0.754	0.15	1.29
	Instantaneous	0.176	0.043	−0.861	1.056		
	Overstress	0.081	0.024	−0.346	0.302		

spontaneous stress to calculate the parameters of the overstress, i.e., $C_5^{(\mathrm{OE})}$, $C_3^{(\mathrm{OE})}$, $C_4^{(\mathrm{OE})}$, $C_2^{(\mathrm{OE})}$ (see Eqs. (44) and (52)). To calculate the histories of inelastic strain rate and overstress, special treatment of experimental data is required for taking the time derivatives over experimental data points, which usually contain scattering due to noise. Such noises are likely to yield unphysical spikes in the results. In order to reduce scattering of experimental data, either a moving averaging technique or fitting a polynomial function prior to making the derivative operation can be adopted. The present work chooses the former one to smoothen the noises and thereby assessing the real material phenomena. All calculations were done using Mathematica© (Wolfram, 1999). Fig. 14 presents the time histories of λ_{1_e} and γ_e obtained from solving Eqs. (44) and (52), respectively, for the relaxation data obtained from HDR. They show an increase in λ_{1_e} and decrease in γ_e with time, owing to progressive stress relaxation. Since, the stress relaxation under simple shear was recorded up to 3600 s, the asymptotic convergence of the γ_e history towards the equilibrium state can be well-noted in Fig. 14(b). The successful application of the moving averaging technique in obtaining the history of $D_{\mathrm{i}12}$ by taking the time derivative of γ_i has been illustrated in Fig. 15. Fig. 16 presents different segments of the histories of $D_{\mathrm{i}11}$ and $D_{\mathrm{i}12}$ (Eqs. (42) and (50)) to manifest the decrease in the inelastic strain rates with the progress of the relaxation process in HDR. Similar results were obtained for NR, but the presentation is being skipped here for space limitation.

Figs. 17 and 18 present the fundamental relation between the Mandel overstress $\hat{\mathbf{P}}_{\mathrm{E}}^{(\mathrm{OE})}$ and the inelastic strain rate $\hat{\mathbf{D}}_{\mathrm{i}}$ for uniaxial compression $(P_{11E}^{(\mathrm{OE})} - D_{\mathrm{i}11})$ and simple shear $(P_{12_{\mathrm{E}}}^{(\mathrm{OE})} - D_{\mathrm{i}12})$. These results were obtained from the relaxation data at different strains (Figs. 4–7) using the proposed identification scheme. The existence of a nonlinear relation can be observed at all cases in HDR and NR. This suggests the necessity of considering the nonlinear dependence of the viscosity in the evolution law (Eq. (35)). The nonlinearity is more prominent when $\hat{\mathbf{D}}_{\mathrm{i}}$ is slower. Furthermore, the relations are found to depend directly on the strain levels of the relaxation experiments.

To formulate an evolution law in a closed form, the stresses $P_{11_{\mathrm{E}}}^{(\mathrm{OE})}$ and $P_{12_{\mathrm{E}}}^{(\mathrm{OE})}$ have been plotted in a form normalized with the overstress values that existed just at the very beginning of the relaxation processes. These normalization stresses depend on the deformation and are denoted as $(\hat{P}_{\mathrm{E}}^{(\mathrm{OE})}|_{\max})$. A physical motivation of this procedure is given by the discussion in Section 2, but we note the existence of a very unique relation for each HDR and NR, in both compression and shear. Figs. 19 and 20 visualize the relations between the normalized overstress $\hat{\mathbf{P}}_{\mathrm{E}}^{(\mathrm{OE})}(t)/\hat{P}_{\mathrm{E}}^{(\mathrm{OE})}|_{\max}$ and $\hat{\mathbf{D}}_{\mathrm{i}}(t)$ for compression, i.e., $P_{11E}^{(\mathrm{OE})}/P_{11E}^{(\mathrm{OE})}|_{\max}$ vs. $D_{\mathrm{i}11}$, and for simple shear, i.e., $P_{12_{\mathrm{E}}}^{(\mathrm{OE})}/P_{12_{\mathrm{E}}}^{(\mathrm{OE})}|_{\max}$ vs. $D_{\mathrm{i}12}$. The plots show good agreement between the data points and the power law functions for all cases except for the case of NR

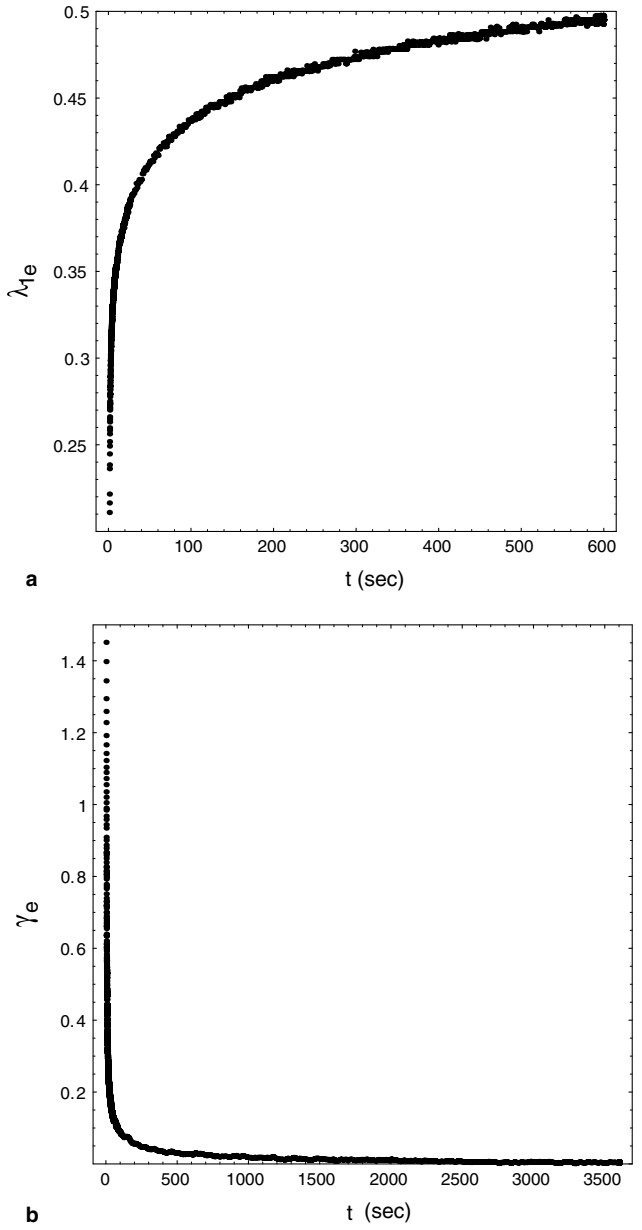

Fig. 14. Elastic strain histories as calculated from the simple relaxation test data of HDR: (a) λ_{1_e} history obtained from simple relaxation test at a stretch level of 0.5; (b) γ_e history obtained from simple relaxation test at a shear strain level of 2.5.

under compression (Fig. 20(a)). Availability of a bit limited number of test data may be one of the reasons for producing such a scatter (Fig. 20(a)). The other possibility of improving the representation is discussed in Section 5.1 together with the simulation results. Yet, all results motivate a power law for describing such relations. In addition,

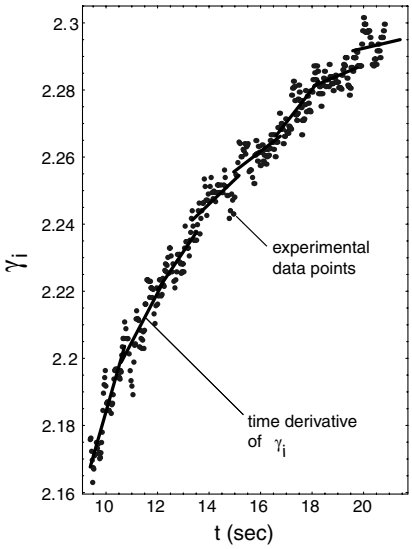

Fig. 15. Inelastic strain history γ_i as calculated from the simple relaxation test data of HDR at 2.5 shear strain level and application of moving averaging method for estimating the time-derivative of inelastic strain γ_i.

a double logarithmic relation may be assumed between the normalization stresses $\hat{P}_E^{(OE)}|_{max}$ recorded at the beginnings of the relaxation histories and the applied strains (see Fig. 21). On the basis of these facts (Figs. 19–21), we propose a constitutive equation for the viscosity of the power law type in general three-dimensional form

$$\hat{\mathbf{D}}_i = \frac{\|\hat{\mathbf{P}}_E^{(OE)}\|^{\delta}}{\eta_0 \pi^{\delta} \cdot \|\mathbf{B}\|^{\varphi}} \cdot \hat{\mathbf{P}}_E^{(OE)}, \tag{54}$$

where δ, φ and η_0 are material parameters to be determined and $\|\mathbf{\Omega}\| = \sqrt{\mathbf{\Omega} \cdot \mathbf{\Omega}}$ is the magnitude of a tensor. The constant π (=1 MPa) is introduced for dimensional reasons. From Eq. (54) we recover the constitutive equation for the nonlinear viscosity in closed form

$$\frac{1}{\eta(\hat{\mathbf{P}}_E^{(OE)}, \mathbf{B})} = \frac{1}{\eta_0} \left(\frac{\|\hat{\mathbf{P}}_E^{(OE)}\|}{\pi} \right)^{\delta} \|\mathbf{B}\|^{-\varphi}. \tag{55}$$

We note that the dependence of the viscosity function η on the left Cauchy Green tensor $\mathbf{B}$ in Eq. (55) is similar to the suggestion provided in Haupt and Sedlan (2001). However, in comparison with the earlier work where an inverse dependence of η on the total strain rate $\mathbf{D}$ was chosen, the current work introduces the overstress $\hat{\mathbf{P}}_E^{(OE)}$ as variable in the evolution equation. The relation proposed here can be incorporated in the constitutive model (Section 3) to derive a rate-dependent model with a nonlinear viscosity function. To estimate the material parameters of the viscosity specified by Eqs. (54) and (55) a least-square method can be applied using the data of $\hat{\mathbf{P}}_E^{(OE)}/\hat{P}_E^{(OE)}|_{max}$ and $\hat{\mathbf{D}}_i$ (Figs. 19 and 20). Table 2 presents the identified values of the parameters for HDR and NR. The parameters

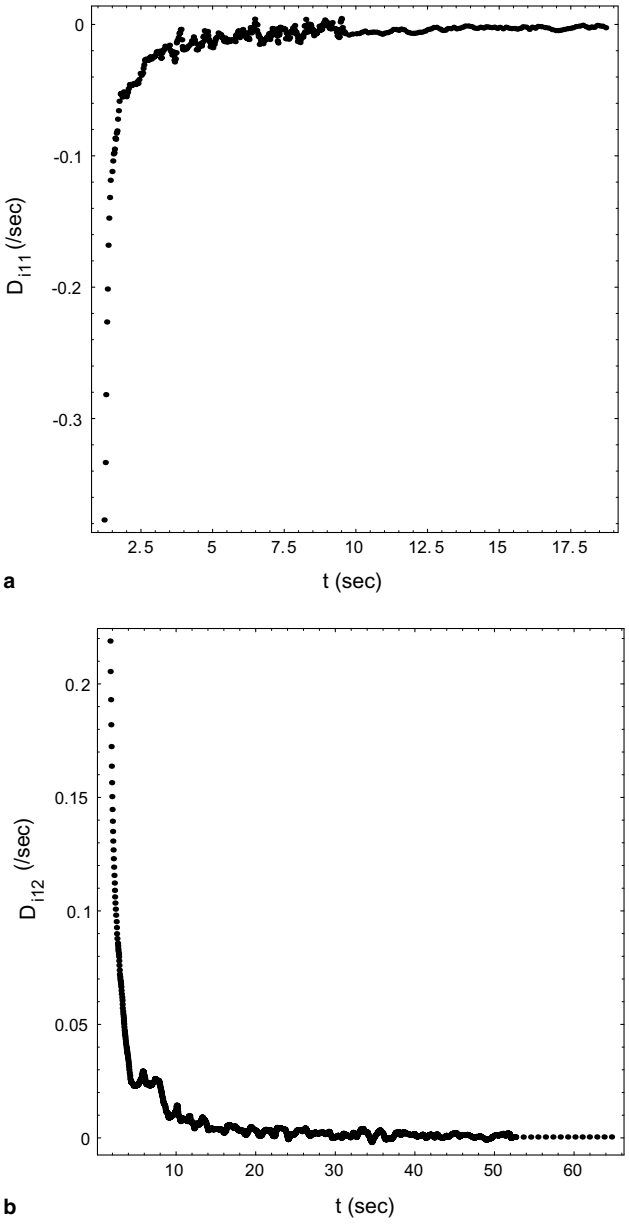

Fig. 16. History of inelastic strain rate as calculated from the simple relaxation test data of HDR: (a) D_{i11} history obtained from simple relaxation test at a stretch level of 0.5; (b) D_{i12} history obtained from simple relaxation test at a shear strain level of 2.5.

describe both the stress and the strain dependence of the positive viscosity, hence consistent with thermodynamic requirements. These parameters along with the elasticity parameters will be used in Section 5 to study the performance of the model in simulating stress responses to strain processes.

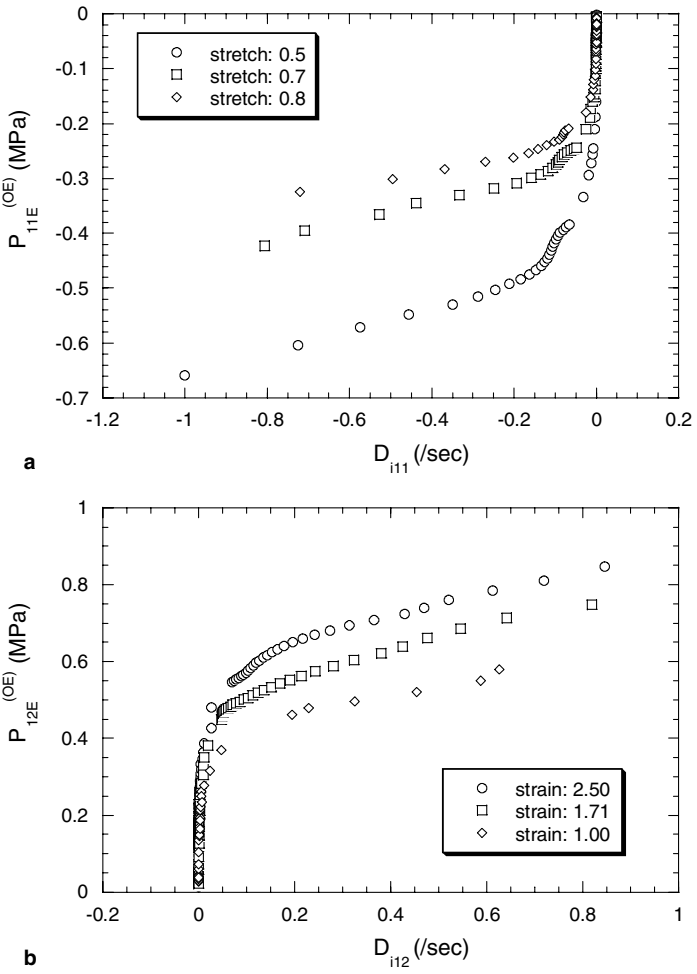

Fig. 17. $\hat{\mathbf{D}}_i$ vs. $\hat{\mathbf{P}}_E^{(OE)}$ relations in one dimension as calculated from simple relaxation test data of HDR: (a) compression; (b) simple shear.

4.3. Extension of the evolution equation for incorporating weak-rate dependency during unloading

The test data shown in Figs. 2 and 3 are considered again with regard to the unloading behavior of HDR and NR. There, although strong rate dependence was observed during the loading phase, weaker rate dependence was found during unloading. All cyclic tests under both compression and shear show this fact. To describe this within the developed model, a smaller viscosity is needed during unloading than during loading. This section describes a possibility of modeling the response of HDR under cyclic compression and shear. The approach is based on the assumption that there exists a general constitutive equation for the viscosity which is valid in both loading and unloading. The total stress power $\mathbf{S} \cdot \mathbf{D}$ is applied to decide between loading and unloading and a tangent hyperbolic

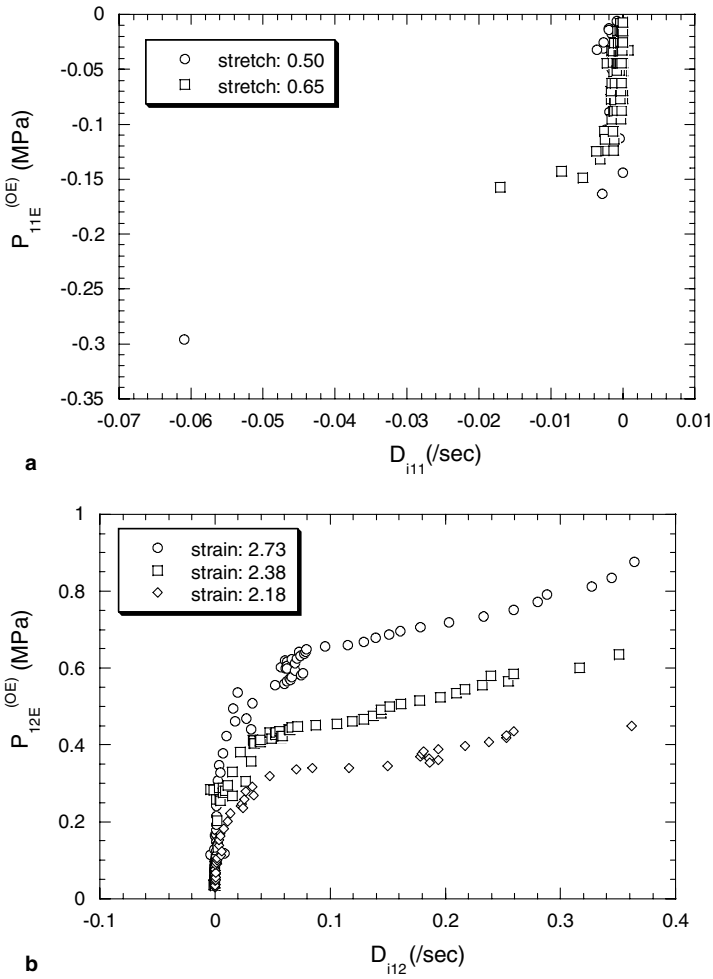

Fig. 18. $\hat{\mathbf{D}}_{\mathrm{i}}$ vs. $\hat{\mathbf{P}}_{\mathrm{E}}^{(\mathrm{OE})}$ relations in one dimension as calculated from simple relaxation test data of NR: (a) compression; (b) simple shear.

function can be employed to assure a very low rate dependence during unloading. The modified constitutive equation for the viscosity is therefore expressed as

$$\eta = \left\{ \eta_1 + (\eta_0 - \eta_1)\frac{1}{2}\{1 + \tanh\{\xi \mathbf{S}\cdot\mathbf{D}\}\} \right\} \frac{\pi^{\delta}\|\mathbf{B}\|^{\varphi}}{\|\hat{\mathbf{P}}_{\mathrm{E}}^{(\mathrm{OE})}\|^{\delta}}. \tag{56}$$

To represent the difference in rate dependence between loading and unloading we take the choice of $\eta_0 \gg \eta_1 \cdot \xi$ is another material parameter that determines the influence of the stress power $\mathbf{S}\cdot\mathbf{D}$. For $\xi\mathbf{S}\cdot\mathbf{D} \gg 0$ we have $\tanh(\xi\mathbf{S}\cdot\mathbf{D}) \approx 1$ and for $\xi\mathbf{S}\cdot\mathbf{D} \ll 0$ we have $\tanh(\xi\mathbf{S}\cdot\mathbf{D}) \approx -1$. The other parameters are those as defined for the simulation of monotonic processes. This is a further generalization of the earlier concept (Section 4.2) where only the loading cases were represented. Some qualitative numerical calculations in the compression and shear regimes are presented in the following section.

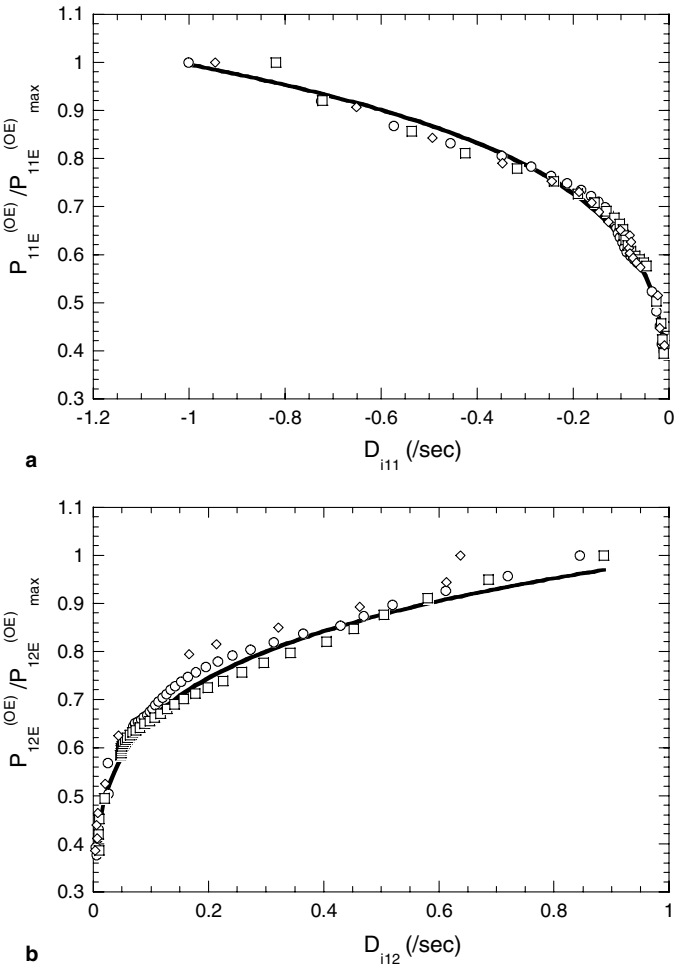

Fig. 19. $\hat{\mathbf{D}}_i$ vs. $\hat{\mathbf{P}}_E^{(OE)}/\hat{P}_E^{(OE)}|_{max}$ relations in one dimension as calculated from simple relaxation test data of HDR: (a) compression; (b) simple shear. The solid line is the path of a best-fit curve defined by a power law, $y = Ax^n$.

5. Numerical simulation

The experiments presented in Section 2 revealed viscosity-induced rate-dependent effects in HDR and NR under compression and shear. A model of finite viscoelasticity was formulated in Section 3 along with proposals to generalize it with an improved hyperelasticity relation and a nonlinear equation for the viscosity in a thermodynamically consistent way. A new method to examine and identify the dependence of the viscosity on the process variables by using one-dimensional relaxation data has been presented in Section 4. The application of this method has motivated a physically nonlinear constitutive equation for the viscosity in a three-dimensional form. In this section, this relation is inserted into the finite strain model (Section 3) to investigate the properties of the whole constitutive theory and the identified parameters (Tables 1 and 2) in simulating relaxation tests at

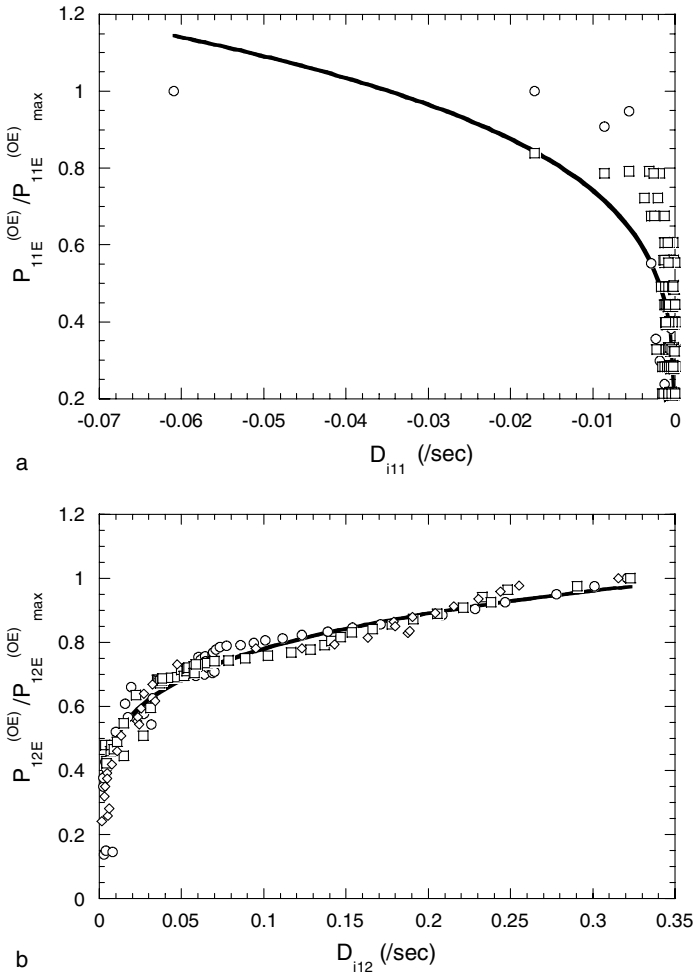

Fig. 20. $\hat{\mathbf{D}}_i$ vs. $\hat{\mathbf{P}}_E^{(OE)}/\hat{P}_E^{(OE)}|_{max}$ relations in one dimensions as calculated from simple relaxation test data of NR: (a) compression; (b) simple shear. The solid line is the path of a best-fit curve defined by a power law, $y = Ax^n$.

different strains. The simulations of multi-step relaxation, monotonic and cyclic tests and as well as their comparison with experiments follow next.

5.1. Relaxation tests

Figs. 22 and 23 present the simulated stress responses of simple relaxation experiments in compression and simple shear regimes on HDR and NR. The results (Figs. 22(a) and (b) and 23(b)) are compared very closely with the experiments in representing the instantaneous responses and equilibrium states that the specimens encounter at the beginning and the end of the relaxation processes. However, as we see in Fig. 23(a), the agreement between experiment and simulation in the short time range is not so well. This agrees with the findings of Fig. 20(a). To improve the representation in this range, we plan to carry out

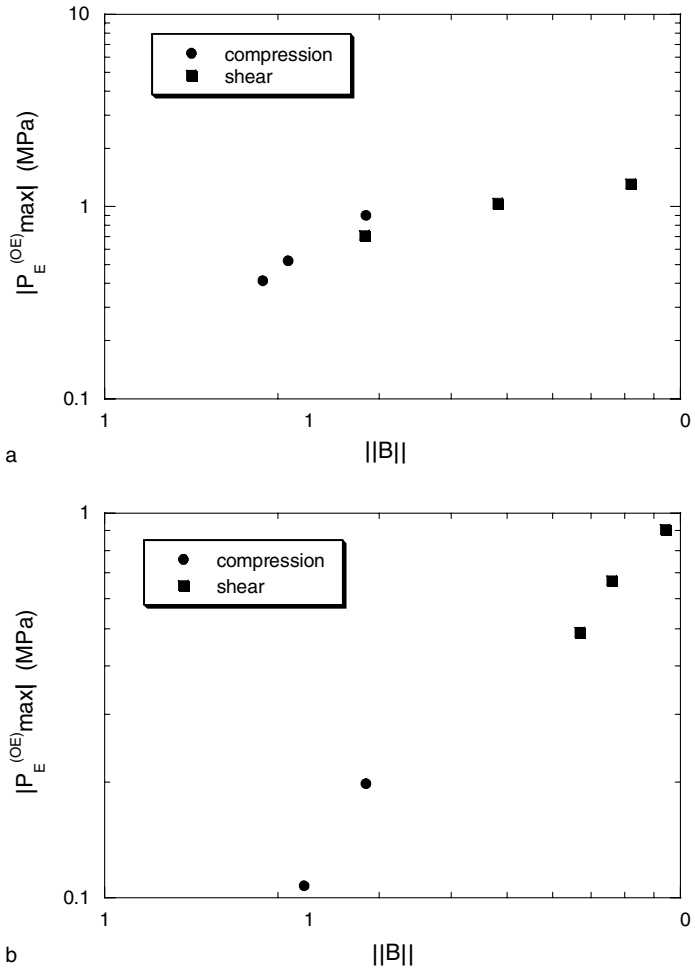

Fig. 21. $\|\mathbf{B}\|$ vs. $|\hat{P}_{E}^{(OE)}{}_{max}|$ relations as calculated from simple relaxation test data of in compression and simple shear: (a) HDR; (b) NR.

Table 2
Viscosity parameters

Specimens	η_0 (MPa s)	δ	ϕ
HDR	1.63	1.46	2.29
NR	2.46	0.78	2.16

the parameter identification by using the time derivative of the stress in a future project. Another possibility is to introduce weighting factors in the error norm which is used in the identification procedure. Furthermore, the stress relaxation over the whole experimentally recorded time range, 600 s for compression and 3600 s for shear, is described in a very promising way. Thus, the enhanced capability of the proposed nonlinear viscosity model and the parameters in comparison with the earlier linear model (Amin et al., 2002) is

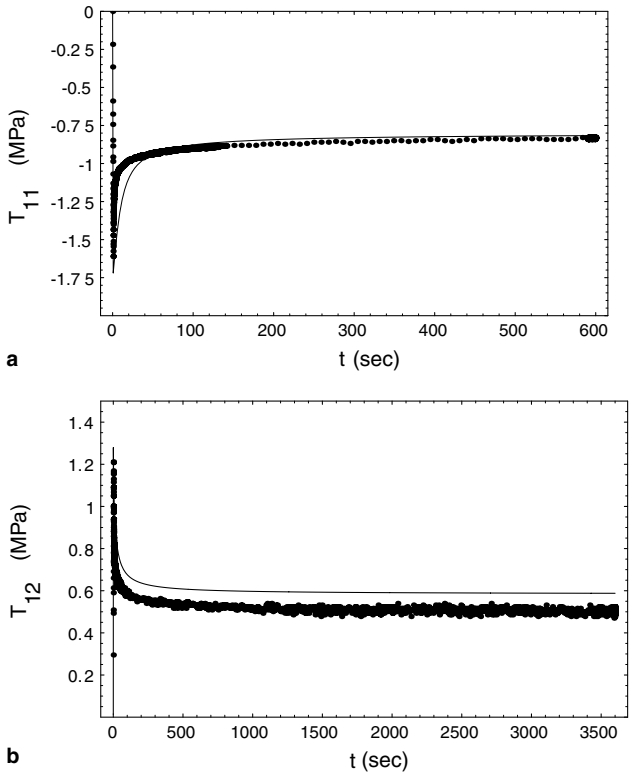

Fig. 22. Numerical simulation of simple relaxation test of HDR. The figures show the simulated stress histories: (a) at 0.7 stretch; (b) at 1.00 shear strain: (−) numerical simulation, (•) experiment.

clearly demonstrated. With the linear model, it was possible to describe the relaxation to a maximum of only up to 50 s for HDR and 10 s for NR. The simulations of the evolution of the viscosity η with changes in $\|\hat{\mathbf{P}}_{\mathrm{E}}^{(\mathrm{OE})}\|$ (Eq. (55)) in simple relaxation tests at different strains (Figs. 4–7) are shown in Figs. 24 and 25, respectively, for HDR and NR. The strong nonlinearity in the evolution of η with increasing $\|\hat{\mathbf{P}}_{\mathrm{E}}^{(\mathrm{OE})}\|$ and $\mathbf{B}$ can be noted for HDR under shear in Fig. 24(b) whereas Fig. 25(a) reveals a contrast phenomenon for NR under compression with a much weaker nonlinearity. In general, the nonlinearity in the evolution of the viscosity as revealed from the simulations (Figs. 24 and 25) is found to be much stronger under shear than that under compression.

At this stage, the capability of the constitutive model to represent process-dependent viscosity effects will be examined by simulating multi-step stress relaxations. Figs. 26 and 27 compare the experimental relaxation curves with the simulated ones for HDR and NR. The long-term relaxation behavior is well described by the theory but in the short-term range there are differences. Since the instantaneous response of the overstress is underestimated, it can be assumed that there are thixotropic recovery effects in the material which correspond to a process-dependent viscosity with its own time scale. In the developed theory, the viscosity depends only on the current deformation and overstress, but a process-dependent viscosity would depend on additional internal variables. If the

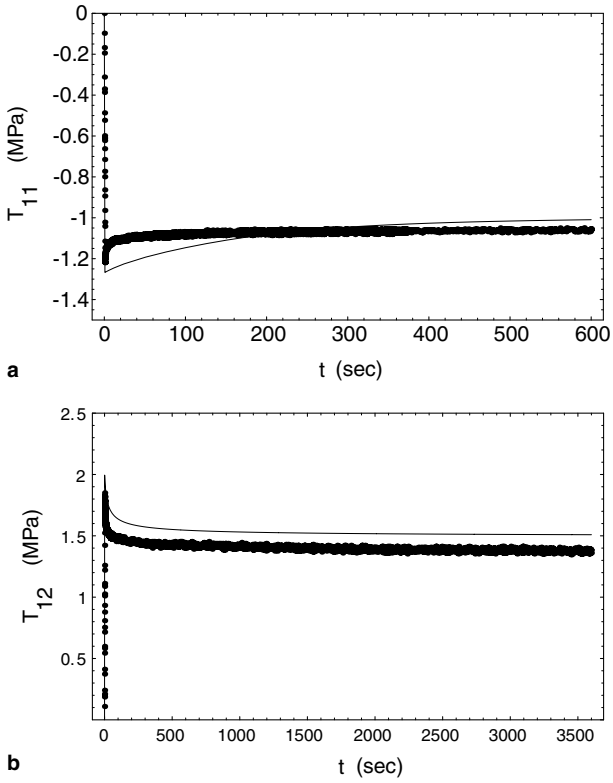

Fig. 23. Numerical simulation of simple relaxation test of NR. The figures show the simulated stress histories: (a) at 0.65 stretch; (b) at 2.18 shear strain: (−) numerical simulation, (•) experiment.

viscosity function would have its own recovery behavior, it becomes larger during the relaxation periods and thus leads to larger overstresses in the short term range of the next relaxation event. A further argumentation can be founded on the introduction of an additional Maxwell element in the constitutive model with a much smaller relaxation time. Concerning the discrepancies between simulation and test more experimental data is needed to understand the process dependence of relaxation behavior and to develop corresponding models.

5.2. Monotonic tests

The capability of the theory to simulate the rate-dependent monotonic response of HDR and NR is examined in Figs. 28 and 29 by comparing the numerical results with experimental data. The comparison shows an excellent correlation between simulation and experiments for slow and fast strain rates in both compression and shear deformation ranges. In general, the accuracy in predicting the experimental response was found to be better under compression than under shear; and also in NR than in HDR. This observation correlates with the results presented in Figs. 24 and 25 where the strongest nonlinearity of the viscosity function was found to exist in HDR under simple shear (Fig. 24(b)). The nonlinearity of the viscosity was found to be the weakest in NR under compression

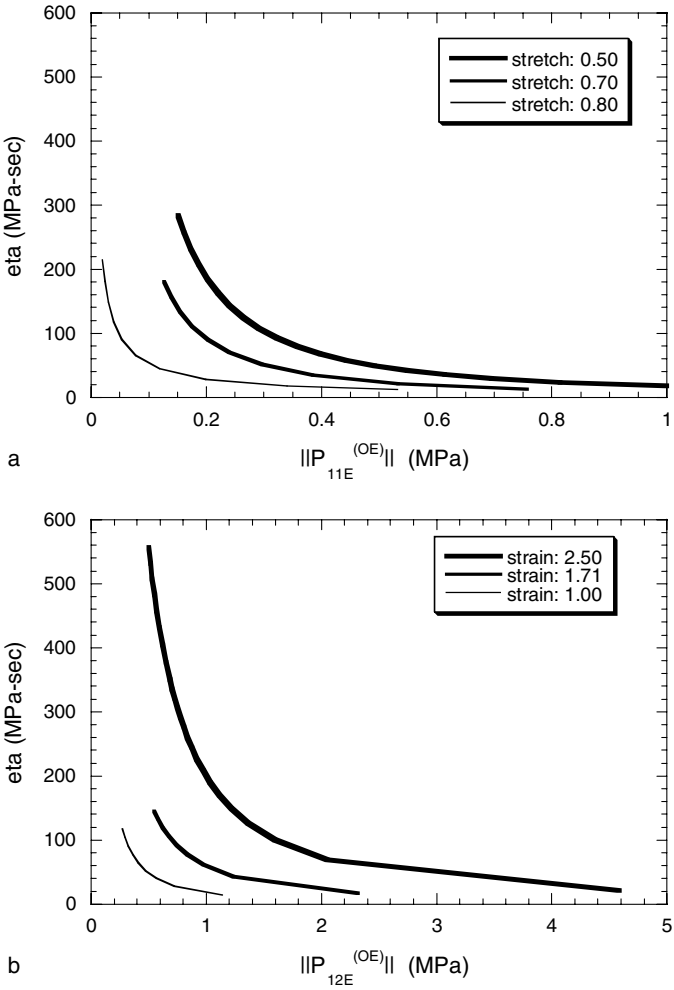

Fig. 24. Nonlinear dependence of viscosity function, η with norm of overstress, $\|\hat{\mathbf{P}}_{\mathrm{E}}^{(\mathrm{OE})}\|$ as obtained from the simulation results of simple relaxation tests at different strain levels on HDR: (a) compression; (b) simple shear.

(Fig. 25(a)). Yet, all simulated responses are found to well describe the rate-dependent monotonic response at low, moderate and large strains along with the representation of high initial stiffness values at low strains, observed especially in HDR. Furthermore, the asymptotic convergence property of the model towards the instantaneous state with increasing strain rate is clearly visible in Fig. 28(a) for HDR under compression. A similar behavior is observed in the other cases, but the presentation of those results is omitted for space limitation. In comparison with the model with a constant viscosity (Amin et al., 2002), a significant improvement in the stress representation for very slow strain rates can be noted. This demonstrates the improvement achievable in monotonic response prediction by considering nonlinear viscosity phenomena in the constitutive model. In addition, we note the reasonable adequacy of the respective set of viscosity parameters for

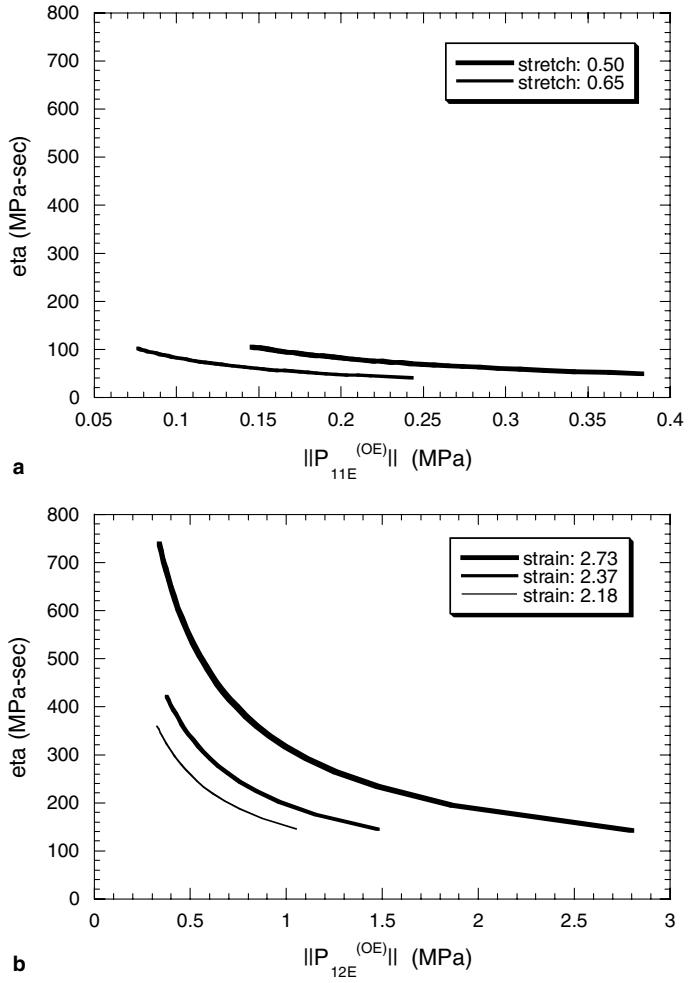

Fig. 25. Nonlinear dependence of viscosity function, η with norm of overstress, $\|\hat{\mathbf{P}}_{\mathrm{E}}^{(\mathrm{OE})}\|$ as obtained from the simulation results of simple relaxation tests at different strain levels on NR: (a) compression; (b) simple shear.

HDR and NR identified from independent simple relaxation tests in predicting rate-dependent monotonic responses as well. Not to mention, the relaxation and monotonic tests on each material were conducted in two different experimental set-ups, e.g., uniaxial compression and simple shear (Section 2). Thus, the developed constitutive theory with its nonlinear viscosity function demonstrates its physical and general sense. Nevertheless, due to power law-based compact nature of the evolution equation, the number of viscosity parameters is quite low, thus offering a notable simplicity in parameter estimation efforts.

5.3. Cyclic tests

One approach to generalize the constitutive equation of the nonlinear viscosity function (Eq. (55)) to represent the experimentally observed cyclic stress responses is presented in

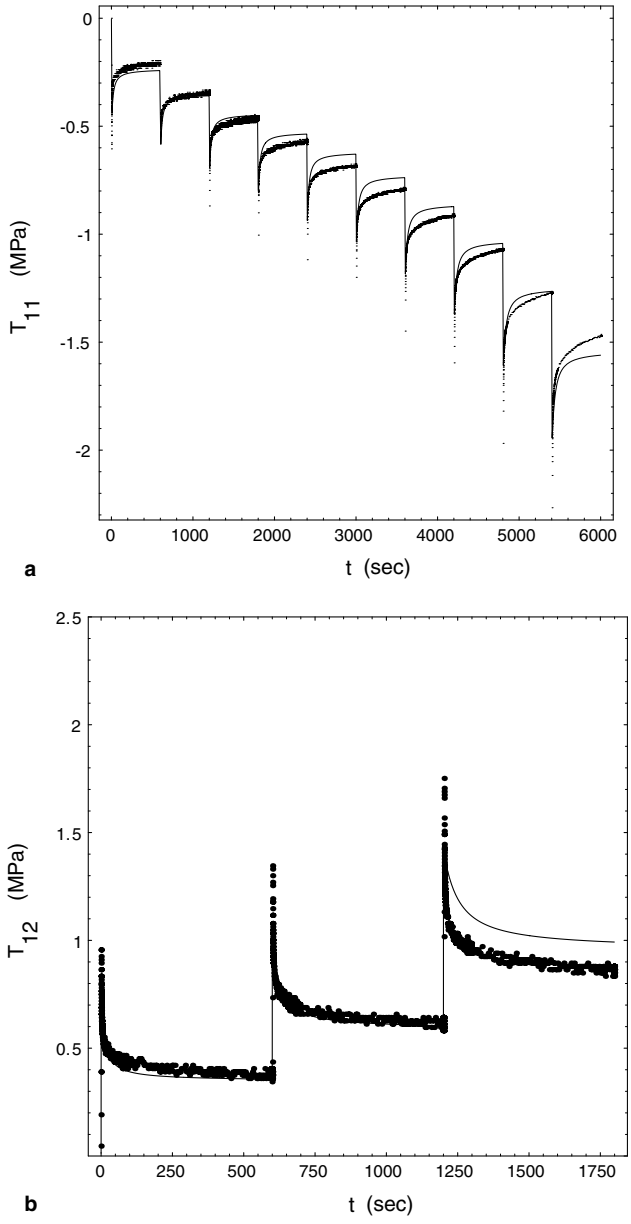

Fig. 26. Numerical simulation of multi-step relaxation test of HDR. The figures show the stress history: (a) compression; (b) simple shear: (−) numerical simulation, (•) experiment.

Section 4.3 (Eq. (56)). The capability of this approach is investigated in this section for HDR. In Fig. 30 two experimental loading and unloading tests under compression with different strain rates are compared with the simulations. The main effect of interest is the pronounced difference in rate sensitivity during loading and unloading which occurs in many polymers (see also Bergström and Boyce, 1998; Khan and Zhang, 2001). The

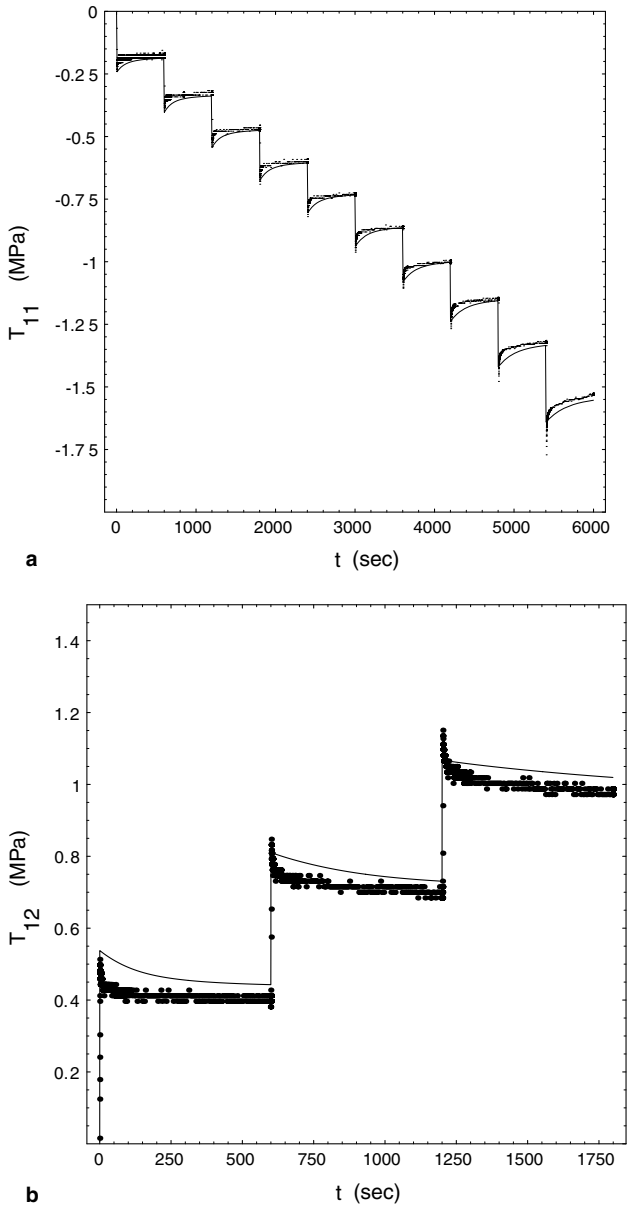

Fig. 27. Numerical simulation of multi-step relaxation test of NR. The figures show the stress history: (a) compression; (b) simple shear: (−) numerical simulation, (•) experiment.

proposed theory has successfully modeled this behavior. Since the hysteresis of the equilibrium response is not considered in the model, permanent set is underestimated. Hence, it can be expected that an additional Maxwell element with a constant viscosity would improve the quality of representation. In Fig. 31 two symmetrical shear tests with different rates are shown and compared with the corresponding simulations. The investigated

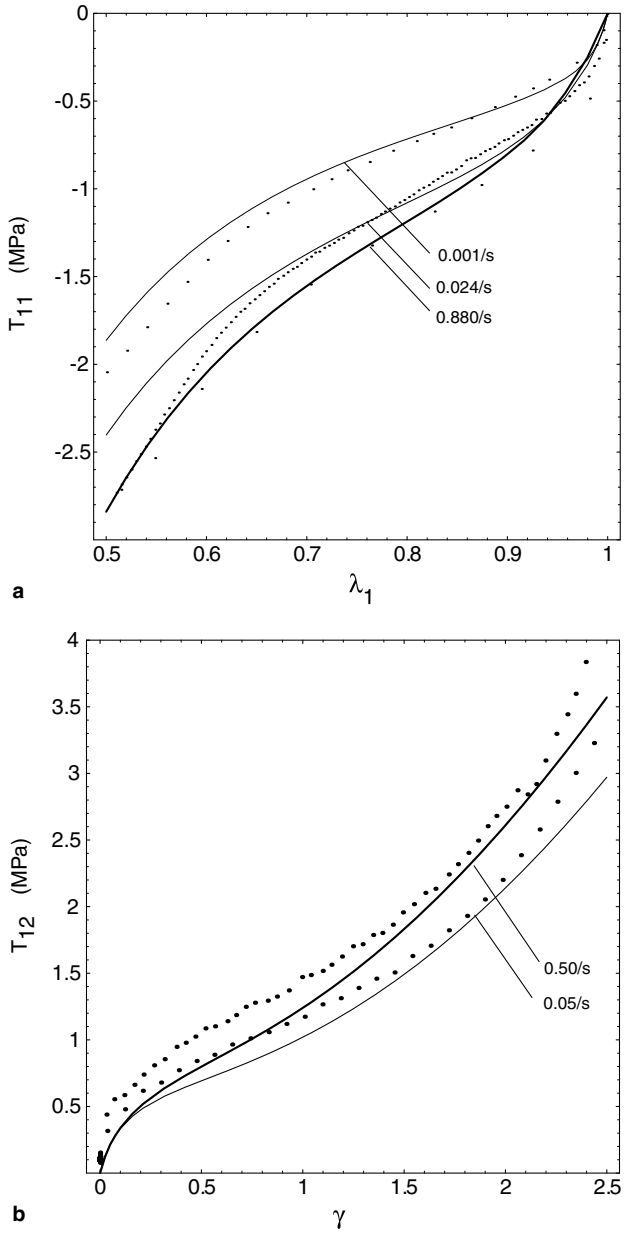

Fig. 28. Numerical simulation of monotonic compression tests of HDR at different strain rates. The figures show the stress–strain responses: (a) compression; (b) simple shear: (–) numerical simulation, (•) experiment.

elastomer shows a pronounced rate sensitivity during loading in shear and a less one during unloading which is described by the model. The amount of hysteresis is underestimated which is similar to the case under compression. Thus, it can be summarized that many effects of HDR are well understood and can be described by the model but there are also

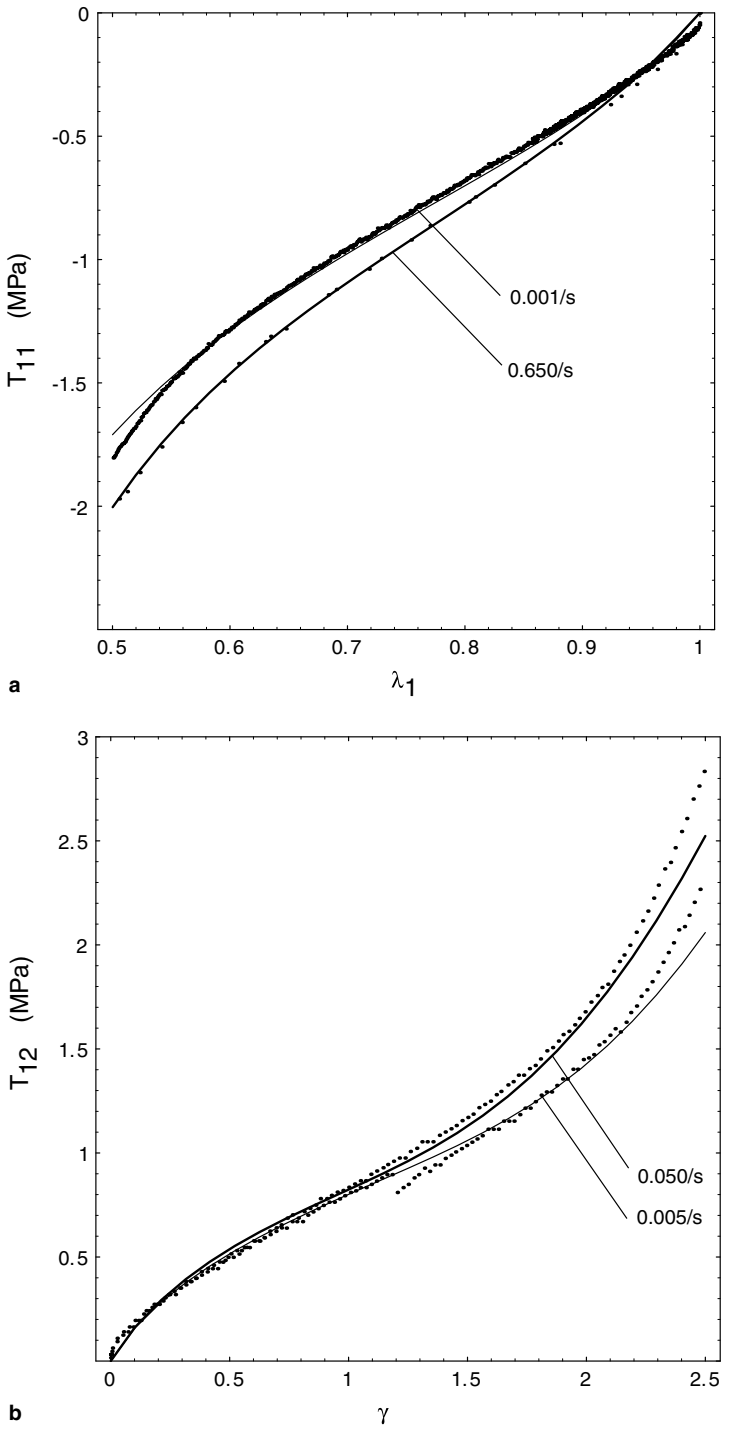

Fig. 29. Numerical simulation of monotonic compression tests of NR at different strain rates. The figures show the stress–strain responses: (a) compression; (b) simple shear: (−) numerical simulation, (•) experiment.

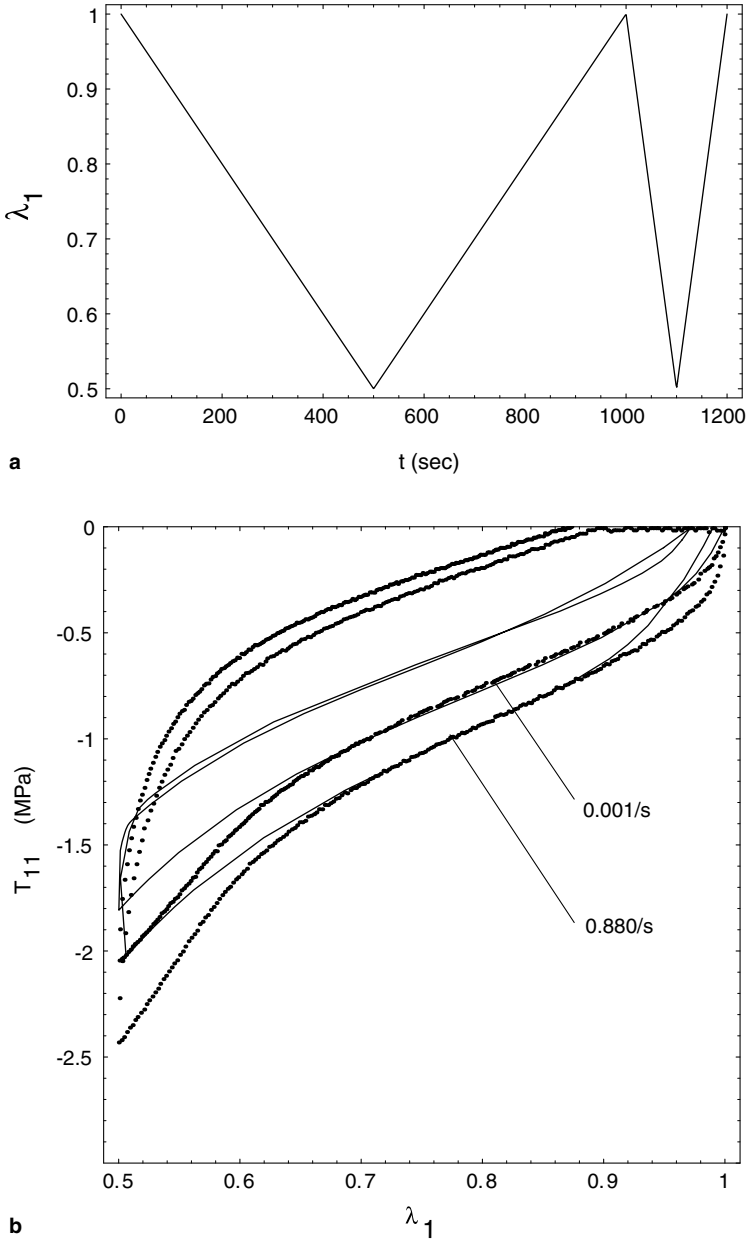

Fig. 30. Numerical simulation of cyclic compression tests of HDR at different strain rates. The simulations are conducted with $\eta_1 = 0.005\eta_0$ and $\xi = 3000$, see Eq. (56): (a) applied stretch history; (b) stress-stretch response: (−) numerical simulation, (•) experiment.

many others, where the proposed constitutive approach has to be improved. The approach of rate-independent elastoplasticity (e.g., Yoshida et al., 2004) can represent stress–strain curves with constant rate, but neither relaxation nor creep or rate-dependence phenomena

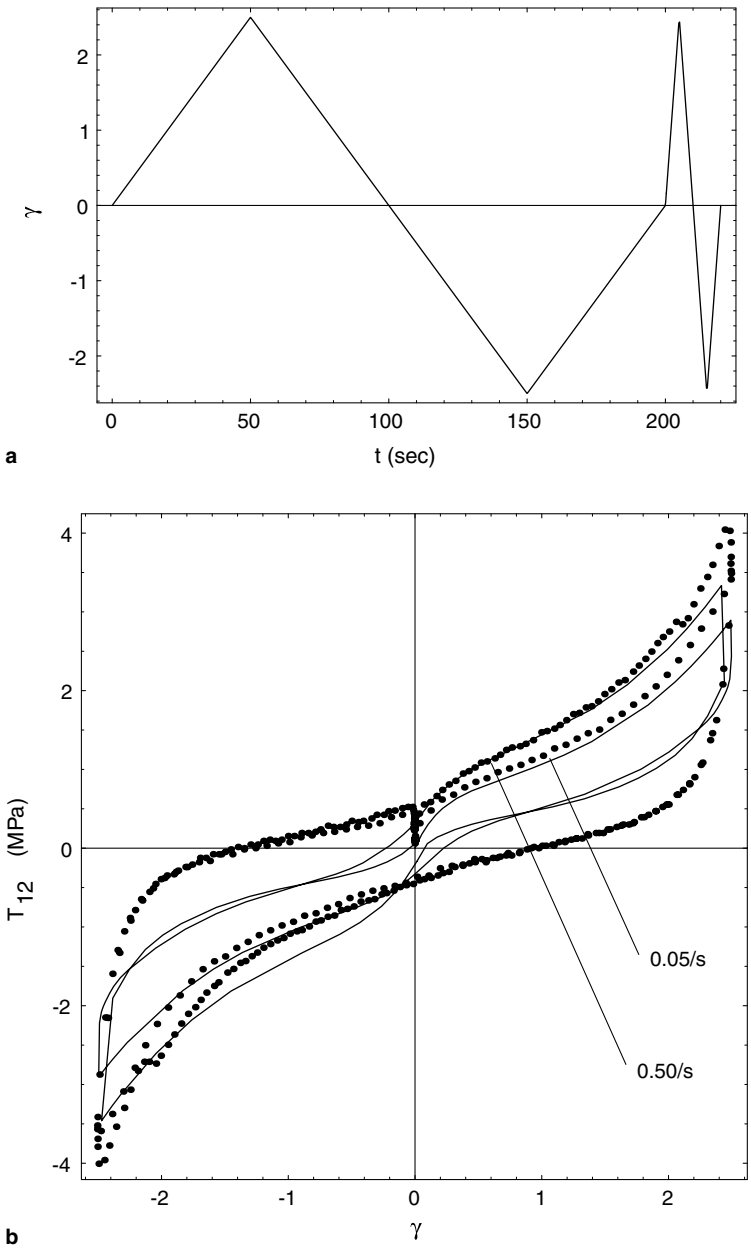

Fig. 31. Numerical simulation of cyclic shear tests of HDR at different strain rates. The simulations are conducted with $\eta_1 = 0.001\eta_0$ and $\xi = 100$, see Eq. (56): (a) applied stretch history; (b) stress-stretch response: (−) numerical simulation, (•) experiment.

can be described. From our point of view, the approach of modeling rubber with plasticity models as applied by Yoshida et al. (2004) describes stress strain curves under constant rates but the physical basis with respect to the thermodynamic consistency is missing.

6. Conclusions

Under both cyclic compression and shear, HDR and NR exhibit significant rate-dependent phenomena in the loading phase whereas during unloading the rate-dependence is very weak. Furthermore, the characterization of viscosity-induced rate-dependent phenomena through simple relaxation experiments shows a very fast stress decay at the very beginning of the relaxation process followed by a very slow decay in the long-term range. These observations provide a motivation to consider the nonlinear dependence of the viscosity in modeling the rate-dependent behavior of HDR and NR. To this end, a finite strain viscoelasticity theory based on a multiplicative splitting of the deformation gradient $\mathbf{F}$ into elastic $\mathbf{F}_e$ and inelastic $\mathbf{F}_i$ parts is developed. The relation between the inelastic strain rate $\hat{\mathbf{D}}_i$ and the overstress $\hat{\mathbf{P}}_E^{(OE)}$ describes the viscosity phenomena. Since the second law of thermodynamics only requires the viscosity η to be a positive quantity, there is a possibility to express the flow rule in a general but thermodynamically consistent form by considering a nonlinear dependence of η on other process quantities or internal variables. Yet, to maintain the physical meaning of the flow rule, it is preferable to make such a generalization based on clear experimental evidences. In this context, it is possible to employ an analytical scheme founded on the basis of the multiplicative split of deformation gradient $\mathbf{F}$ to analyze the data obtained from stress relaxation experiments and thereby evaluating the fundamental $\hat{\mathbf{D}}_i$ vs. $\hat{\mathbf{P}}_E^{(OE)}$ relation for one-dimensional cases. To reduce the scattering of the numerically differentiated experimental data in this process, the moving averaging technique was applied. Since this technique does not eliminate all these oscillations, it should be better to smooth the overall signals by fitting an appropriate function on it, for example, an exponential function or a power law. The evaluation conducted in this paper suggests the dominance of the 'overstress values that existed just at the very beginning of the relaxation process' $\hat{P}_E^{(OE)}|_{max}$ in the stress relaxation process for both HDR and NR under compression and shear. Furthermore, the existence of a relation between $\hat{\mathbf{P}}_E^{(OE)}|_{max}$ and the magnitude of deformation $\|\mathbf{B}\|$ is also evident. Thus, it is possible to identify a nonlinear constitutive relation for the viscosity which is based on two power laws for the investigated rubbery materials. The finite strain viscoelasticity model with a nonlinear equation for the viscosity maintains a compact and simple form. It is conceptually similar to the standard three parameter solid or the Zener model (Fig. 1) involving only three material constants. Numerical simulation of monotonic deformation processes with different strain rates, simple relaxation and multi-step relaxation tests have illustrated the adequacy of the model and the identified parameters in physical and general senses. Although the analytic approach to evaluate the stress relaxation data to identify the evolution law for the viscosity has been utilized in this literature only for HDR and NR, we believe that this technique is conceptually applicable for other solids under finite and small strains as well. Furthermore, the stress power $\mathbf{S} \cdot \mathbf{D}$ can be utilized as a continuous measure for the degree of loading–unloading while the tangent hyperbolic function can be used to represent a strong rate dependence during loading and a weak rate-dependency during the unloading phase of a cyclic process.

Acknowledgements

The authors are indeed grateful to Professor H. Horii, Department of Civil Engineering, University of Tokyo, Japan for his valuable comments and particularly for extending

the experimental facilities of his laboratory to carry out the mechanical tests of this investigation. The authors gratefully acknowledge the kind cooperation extended by the Yokohama Rubber Co. by providing test specimens. The authors also sincerely recall the funding provided by the Japanese Ministry of Education, Science, Sports and Culture as Grant-in-Aid for Scientific Research (C) (No. 12650457) to carry out this research. Dr. A.F.M.S. Amin is grateful to the German Academic Exchange Service (Deutscher Akademischer Austausch Dienst, DAAD) for the fellowship for the stay at the University of Kassel, Germany as a Visiting Professor and also to Professor A. Matzenmiller, Institute of Mechanics, University of Kassel, Germany for encouraging discussions that helped towards the finalization of this work.

References

AASHTO, 1992. Standard Specifications for Highway Bridges, 15th ed. American Association for State Highway and Transportation Officials, Washington, DC.

Amin, A.F.M.S., 2001. Constitutive Modeling for Strain-rate Dependency of Natural and High Damping Rubbers. Doctoral Dissertation, Saitama University, Japan.

Amin, A.F.M.S., Alam, M.S., Okui, Y., 2002. An improved hyperelasticity relation in modeling viscoelasticity response of natural and high damping rubbers in compression: experiments, parameter identification and numerical verification. Mech. Mater. 34, 75–95.

Amin, A.F.M.S., Alam, M.S., Okui, Y., 2003. Measurement of lateral deformation of natural and high damping rubbers in large deformation uniaxial tests. J. Test. Eval., ASTM 31 (6), 524–532.

Amin, A.F.M.S., Wiraguna, S.I., Bhuiyan, A.R., Okui, Y., 2006. Hyperelasticity model for FE analysis of natural and high damping rubbers in compression and shear. J. Eng. Mech., ASCE 132 (1), 1–11.

Ball, R.C., Doi, M., Edwards, S.F., Warner, M., 1981. Elasticity of entangled networks. Polymer 22, 1010–1018.

Bardenhagen, S.G., Stout, M.G., Gray, G.T., 1997. Three-dimensional, finite deformation, viscoplastic constitutive models for polymeric materials. Mech. Mater. 25, 235–253.

Bergström, J.S., Boyce, M.C., 1998. Constitutive modeling of the large strain time-dependent behavior of elastomers. J. Mech. Phys. Solids 46, 931–954.

Bergström, J.S., Boyce, M.C., 2000. Large strain time-dependent behavior of filled elastomers. Mech. Mater. 32, 627–644.

Besdo, D., Ihlemann, J., 2003a. Properties of rubberlike materials under large deformations explained by self organizing linkage patterns. Int. J. Plasticity 19, 1001–1018.

Besdo, D., Ihlemann, J., 2003b. A phenomenological constitutive model for rubberlike materials and its numerical applications. Int. J. Plasticity 19, 1019–1036.

Bonet, J., 2001. Large strain viscoelastic constitutive models. Int. J. Solid Struct. 38, 2953–2968.

Boyce, M.C., Arruda, E.M., 2000. Constitutive models of rubber elasticity: a review. Rubber Chem. Technol. 73, 504–523.

Bueche, F., 1961. Mullins effect and rubber–filler interaction. J. Appl. Polym. Sci. 5, 271–281.

Carr, A.J., Cooke, N., Moss, P.J., 1996. Compression behavior of bridge bearings used for seismic isolation. Eng. Struct. 18, 351–362.

Castellani, A., Kajon, G., Panjeri, P., Pezzoli, P., 1998. Elastomeric materials used for vibration isolation of railway lines. J. Eng. Mech. 124, 614–621.

Charlton, D.J., Yang, J., Teh, K.K., 1994. A review of methods to characterize rubber elastic behavior for use in finite element analysis. Rubber Chem. Technol. 67, 481–503.

Christensen, R.M., 1980. A nonlinear theory of viscoelasticity for application to elastomers. J. Appl. Mech. 47, 762–768.

Colak, C.O., 2005. Modeling deformation behavior of polymers with viscoplasticity theory based on overstress. Int. J. Plasticity 21, 145–160.

Coleman, B.D., Gurtin, M.E., 1967. Thermodynamics with internal state variables. J. Chem. Phys. 47 (2), 597–613.

Coleman, B.D., Noll, W., 1960. An approximation theorem for functionals with application in continuum mechanics. Arch. Rat. Mech. Anal. 6, 355–370.

Coleman, B.D., Noll, W., 1961. Foundations of linear viscosity. Rev. Modern Phys. 33 (2), 239–249.

Dannis, M.L., 1962. Stress–strain testing of rubbers at high rates of elongation. J. Appl. Polym. Sci. 6, 283–296.
Dorfmann, A., Burtscher, S.L., 2000. Aspects of cavitation damage in seismic bearings. J. Struct. Eng., ASCE 126, 573–579.
Drozdov, A.D., 1997. A constitutive model for nonlinear viscoelastic media. Int. J. Solids Struct. 34, 2685–2707.
Drozdov, A.D., Dorfmann, A., 2003. A micro-mechanical model for the response of filled elastomers and finite strains. Int. J. Plasticity 19, 1037–1067.
European Commission, 1999. Highly Adaptable Rubber Isolating System (HARIS). Final Technical Report. Contract # BRPR-CT95-0072, Project # Be-1258.
Fujita, T., Fujita, S., Tazaki, S., Yoshizawa, T., Suzuki, S., 1990. Research, development and implementation of rubber bearings for seismic isolations. JSME Int. J. 33, 394–403.
Gent, A.N., 1962a. Relaxation processes in vulcanized rubber. I. Relation among stress relaxation, creep, recovery, and hysteresis. J. Appl. Polym. Sci. 6, 33–441.
Gent, A.N., 1962b. Relaxation processes in vulcanized rubber. II. Secondary relaxation due to network breakdown. J. Appl. Polym. Sci. 6, 442–448.
Govindjee, S., Simo, J.C., 1991. A micromechanically based continuum damage model for carbon black filled rubbers incorporating Mullins' effect. J. Mech. Phys. Solids 39, 87–112.
Govindjee, S., Simo, J.C., 1992a. Mullins' effect and strain amplitude dependence of the storage modulus. Int. J. Solid Struct. 29, 1737–1751.
Govindjee, S., Simo, J.C., 1992b. Transition from micro-mechanics to computationally efficient phenomenology: carbon black filled rubbers incorporating Mullins' effect. J. Mech. Phys. Solid 40, 213–233.
Green, M.S., Tobolsky, A.V., 1946. A new approach to the theory of relaxing polymeric media. J. Phys. Chem. 14, 80–92.
Haupt, P., 2000. Continuum Mechanics and Theory of Materials. Springer-Verlag, Berlin.
Haupt, P., Lion, A., 2002. On finite linear viscoelasticity of incompressible isotropic materials. Acta Mech. 159, 87–124.
Haupt, P., Sedlan, K., 2001. Viscoplasticity of elastomeric materials: experimental facts and constitutive modelling. Arch. Appl. Mech. 71, 89–109.
Holzapfel, G.A., 1996. On large strain viscoelasticity: continuum formulation and finite element applications to elastomeric structures. Int. J. Numer. Meth. Eng. 39, 3903–3926.
Holzapfel, G.A., Simo, J.C., 1996. A new viscoelastic constitutive model for continuous media at finite thermomechanical changes. Int. J. Solid Struct. 33, 3019–3034.
Huber, N., Tsakmakis, C., 2000a. Finite deformation viscoelasticity laws. Mech. Mater. 32, 1–18.
Huber, N., Tsakmakis, C., 2000b. Discussion of finite deformation viscoelasticity laws with reference to torsion loading. Continuum Mech. Thermodyn. 12, 303–323.
Johnson, M.A., Beatty, M.F., 1993a. A constitutive equation for the Mullins effect in stress controlled uniaxial extension experiments. Continuum Mech. Thermodyn. 5, 301–318.
Johnson, M.A., Beatty, M.F., 1993b. Mullins effect in uniaxial extension and its influence on transverse vibration of a rubber string. Continuum Mech. Thermodyn. 5, 83–115.
Johnson, A.R., Stacer, R.G., 1993. Rubber viscoelasticity using the physically constrained system's stretches as internal variables. Rubber Chem. Technol. 66, 567–577.
Johnson, A.R., Quigley, C.J., Young, D.G., Danik, J.A., 1993. Viscohyperelastic modeling of rubber vulcanizates. Tire Sci. Technol. 21, 179–199.
Johnson, A.R., Quigley, C.J., Mead, J.L., 1994. Large strain viscoelastic constitutive models for rubber, Part I: Formulations. Rubber Chem. Technol. 67, 904–917.
Kaliske, M., Rothert, H., 1997. Formulation and implementation of three-dimensional viscoelasticity at small and finite strains. Comput. Mech. 19, 228–239.
Kelly, J.M., 1991. Dynamic and Failure Characteristics of Bridgestone Isolation Bearings, Report No. UCB/EERC-91/04.
Kelly, J.M., 1997. Earthquake Resistant Design with Rubber. Springer-Verlag, London.
Khan, A., Zhang, H., 2001. Finite deformation of a polymer: experiments and modeling. Int. J. Plasticity 17, 1167–1188.
Khan, A.S., Lopez-Pamies, O., 2002. Time and temperature dependent response and relaxation of a soft polymer. Int. J. Plasticity 18, 1359–1372.
Kilian, H.G., Strauss, M., Hamm, W., 1994. Universal properties of filler loaded rubbers. Rubber Chem. Technol. 67, 1–16.

Krempl, E., Khan, F., 2003. Rate (time)-dependent deformation behavior: an overview of some properties of metals and solid polymers. Int. J. Plasticity 19, 1069–1095.
Krempl, E., 1987. Models of viscoplasticity: some comments on equilibrium (back) stress and drag stress. Acta Mech. 69, 25–42.
Laiarinandrasana, L., Piques, R., Robisson, A., 2003. Visco-hyperelastic model with internal state variable coupled with discontinuous damage concept under total Lagrangian formulation. Int. J. Plasticity 19, 977–1000.
Leonov, A.I., 1976. Nonequilibrium thermodynamics and rheology of viscoelastic polymer media. Rheologica Acta 15 (2), 85–98.
Lion, A., 1996. A constitutive model for carbon black filled rubber: experimental investigations and mathematical representation. Continuum Mech. Thermodyn. 8, 153–169.
Lion, A., 1997. A physically based method to represent the thermo-mechanical behavior of elastomers. Acta Mech. 123, 1–25.
Lion, A., Kardelky, C., 2004. The Payne effect in finite viscoelasticity constitutive modelling based on fractional derivatives and intrinsic time scales. Int. J. Plasticity 20, 1313–1345.
Lubliner, J., 1969. On fading memory in materials of evolutionary type. Acta Mech. 8, 75–81.
Lubliner, J., 1973. On the structure of the rate equations of materials with internal variables, Acta Mechanica 17, 109–119.
Lubliner, J., 1985. A model for rubber viscoelasticity. Mech. Res. Commun. 12, 93–99.
Lubliner, J., 1986. Normality rules in large-deformation plasticity. Mech. Mater. 5, 29–34.
Makradi, A., Ahzi, S., Gregory, R.V., Edie, D.D., 2005. A two-phase self-consistent model for the deformation and phase transformation behavior of polymers above the glass transition temperature: application to PET. Int. J. Plasticity 21, 741–758.
Mason, P., 1960. The strain dependence of rubber viscoelasticity, Part II. The influence of carbon black. J. Appl. Polym. Sci. 4, 212–218.
Mattheck, C., Erb, D., 1991. Shape optimization of a rubber bearing. Int. J. Fatigue 13, 206–208.
Meinecke, E.A., Taftaf, M.I., 1987. Effect of carbon black on the mechanical properties of elastomers. Rubber Chem. Technol. 61, 534–547.
Miehe, C., Keck, J., 2000. Superimposed finite elastic–viscoelastic–plastoelastic stress response with damage in filled rubbery polymers. Experiments, modeling and algorithmic implementation. J. Mech. Phys. Solids 48, 323–365.
Mooney, M., 1940. A theory of large elastic deformation. J. Appl. Phys. 11, 582–592.
Mori, A., Carr, A.J., Cooke, N., Moss, P.J., 1996. Compression behavior of bridge bearings used for seismic isolation. Eng. Struct. 18, 351–362.
Mullins, L., 1969. Softening of rubber by deformations. Rubber Chem. Technol. 42, 339–362.
Mullins, L., 1987. Engineering with rubber. Chem. Tech., 720–727.
Ogden, R.W., Roxburgh, D.G., 1999. A pseudo-elastic model for the Mullins effect in filled rubber. Proc. Roy. Soc. Lond. A 455, 12861–12878.
Quigley, C.J., Mead, J., 1995. Large strain viscoelastic constitutive models for rubber, Part II: Determination of material constants. Rubber Chem. Technol. 68, 230–247.
Ramberger, G., 2002. Structural bearings and expansion joints for bridges, structural engineering documents 6. International Association for Bridge and Structural Engineering, Zurich, Switzerland.
Reese, S., Govindjee, S., 1998. A theory of finite viscoelasticity and numerical aspects. Int. J. Solid Struct. 35, 3455–3482.
Rivlin, R.S., 1948. Large elastic deformations of isotropic materials: fundamental concepts. Philos. Trans. Roy. Soc. Lond. A 240, 459–490.
Roeder, C.W., Stanton, J.F., 1983. Elastomeric bearings: state-of-the-art. J. Struct. Eng., ASCE 109, 2853–2871.
Seibert, D.J., Schöche, N., 2000. Direct comparison of some recent rubber elasticity models. Rubber Chem. Technol. 73, 366–384.
Sidoroff, F., 1975a. Variables internes en viscoélasticité I. Variables internes scalaires et tensorielles. J. de Mécanique 14 (3), 545–566.
Sidoroff, F., 1975b. Variables internes en viscoélasticité II. Milieux avec configuration intermédiaire. J. de Mécanique 14 (4), 571–595.
Simo, J.C., 1987. On a fully three dimensional finite strain viscoelastic damage model: formulation and computational aspects. Comput. Meth. Appl. Mech. Eng. 60, 153–173.

Sullivan, J.L., Morman, K.N., Pett, R.A., 1979. A nonlinear viscoelastic characterization of a natural rubber gum vulcanizate. Rubber Chem. Technol. 53, 805–822.

Ward, I.M., 1985. Mechanical Properties of Solid Polymers. Wiley, New York, USA.

Wiraguna, S.I., 2003. Mechanical Behavior of High Damping Rubber Under Shear Deformation. M.Sc. Thesis, Saitama University, Japan.

Wischt, C.E., 1998. The Effect of Carbon Black on Elastic and Viscoelastic Properties of Elastomers. Ph.D. Thesis, University of Akron, USA.

Wolfram Research Inc., 1999. Mathematica, Version 4.0, USA.

Yamashita, Y., Kawabata, S., 1992. Approximated form of the strain energy density function of carbon-black filled rubbers for industrial applications. J. Soc. Rubber Ind. (Jpn.) 65 (9), 517–528 (in Japanese).

Yeoh, O.H., 1990. Characterization of elastic properties of carbon-black filled rubber vulcanizates. Rubber Chem. Technol. 63, 792–805.

Yoshida, J., Abe, M., Fujino, Y., 2004. Constitutive modeling for high-damping rubber materials. J. Eng. Mech., ASCE 130, 129–141.